

Numerical Computations For Shear Bands in an Antiplane Shear Model

F. Xabier Garaizar*

Department of Mathematics, Box 8205
North Carolina State University
Raleigh, NC 27695-8205

David G. Schaeffer†

Department of Mathematics, Box 90320
Duke University
Durham, NC 27706-0320

January 24, 1995

Abstract

We study numerically a model for shear bands that is loosely based on antiplane shearing of granular material. In the model, a shear band is idealized to a jump discontinuity in the solution to the dynamic PDE. We do not explicitly incorporate small scale effects within the shear band into the model—rather at the shear band we impose a jump condition which includes a length parameter modeling the grain diameter. At this level of approximation, we study in several cases the process by which shear bands first form and subsequently develop, including the growth of the unloading region containing the shear band(s).

Our computations use a Godunov method, based on solving appropriate Riemann problems. In some cases, depending on the size of the jump, the Riemann problems under study do not admit a similarity solution because scale invariance is violated by the jump condition at the shear band. This novel feature adds mathematical interest to the present computations.

*supported by NSF Grant DMS 9201115

†supported by NSF Grant DMS 9201034

1 Introduction

It is believed that shear bands form in a material when the dynamic partial differential equations in a continuum formulation lose hyperbolicity and become ill-posed (cf MANDEL, 1964; SCHAEFFER, 1990.) More precisely, if one assumes in elastoplasticity that plastic loading continues throughout an entire sample, then at large deformations the dynamic PDE often become ill-posed; i.e., the theory becomes untenable. Shear bands provide the resolution of this difficulty—rather than continuing to load everywhere, plastic deformation localizes to one or more shear bands and the rest of the sample unloads. Shear bands represent a stronger discontinuity than is usual in continuum mechanics - the displacement, not merely the velocity, is discontinuous.

In this paper we study the model (SCHAEFFER, 1992) for shear banding. In this model, which is loosely based on antiplane shearing of granular material, a shear band is idealized to a jump discontinuity in the solution to the dynamic PDE. We do not explicitly incorporate small scale effects within the shear band into the model—rather at the shear band we impose a jump condition which includes a length parameter modeling the grain diameter.

We focus primarily on the initial formation and development of shear bands. When a shear band first forms, simultaneously there appears a region in the material in which loading behavior is replaced by unloading. Initially this region has zero thickness and in fact coincides with the shear band, but it grows as time evolves. In other words, the oversimplified statement above -plastic loading localizes to a shear band and the rest of the sample unloads- may describe the large time behavior, but there is a dynamic process by which this situation is achieved. Since the extent of this unloading region is unknown ‘a priori’, we are dealing with a free boundary problem in which, incidentally, the governing PDE are hyperbolic (regarding unloading waves see also LEE (1953) and CLIFTON and BODNER (1965), CLIFTON and TING (1968), VON KARMAN ET AL. (1943), RAKHMATULIN (1945) and SKOBEEV (1963)).

The main contribution of this paper is to solve numerically the model in several cases involving the formation of shear bands; viz., (i) a Riemann type problem, (ii) uniform loading with one weak spot, and (iii) uniform loading with two weak spots. In case (i), the specific Riemann problem does not admit a similarity solution because scale invariance is violated by the jump condition at the shear band. Analytical results are available for this problem (SCHAEFFER and SHEARER, 1993), and our numerical solution agrees well with them. In case (iii), the competition between the two shear bands which form is the phenomenon of particular interest.

In Sections 2 and 3 of this paper, the model is recalled from SCHAEFFER (1992) and some elementary analysis of it is recalled from GARAIZAR (1993). Our numerical method, a Godunov-type method including ideas from front tracking (CHERN and COLELLA, 1987) is discussed in Section 4. Finally Section 5 presents the results of the

computations. In addition, there are two appendices. The first describes a numerical implementation of the analytical solution used as comparison with the calculations; the second extends the local existence result of SCHAEFFER and SHEARER (1993) to a global one.

2 Continuous solutions

2.1 The model

We consider a model proposed by SCHAEFFER (1992) which is loosely related to antiplane shearing of granular material. However we restrict our attention to solutions depending on one space variable and time (i.e., simple shear). Specifically we study the system of equations

$$\begin{aligned} \partial_t v &= c^2 \partial_x \sigma \\ \partial_t(\sigma + H(\gamma)) &= \partial_x v \\ \partial_t(\tau - \alpha H(\gamma)) &= 0. \end{aligned} \tag{1}$$

where v is the z -component of the velocity vector, and σ and τ are the T_{31} and T_{32} components of the Cauchy stress tensor, T_{ij} . All the other components of the stress tensor and velocity vector vanish. The parameter α relates to the degree of non-associativity in the material, and c is the elastic wave speed¹. As in GARAIZAR (1993), $H(\gamma)$ is interpreted by identifying $H'(\gamma)$ as the reciprocal of the hardening modulus. We assume that $H(\gamma)$ satisfies the monotonicity and convexity conditions $H'(\gamma) \geq 0$ and $H''(\gamma) \geq 0$.

The yield condition here is obtained by approximating the yield surface of SCHAEFFER (1992) by its tangent plane. The yield stress, γ , is considered as a history parameter and is subject to a dynamical evolution

$$\partial_t \gamma = \begin{cases} \partial_t(\sigma + \alpha\tau)|_+ & \text{if } \sigma + \alpha\tau = \gamma \\ 0 & \text{if } \sigma + \alpha\tau < \gamma \end{cases}, \tag{2}$$

where $d|_+ = d$ if $d > 0$ and $d|_+ = 0$ if $d \leq 0$. The yield condition can be expressed in non-differential form as

$$\gamma(x, t) = \max_s \{ \sigma(x, s) + \alpha\tau(x, s) \quad : \quad s \leq t \}.$$

We notice that the system (1)(2) is in conservation form even though the full two dimensional system of SCHAEFFER (1992) is not.

¹More precisely, c is the nondimensionalized wave speed in the scaling introduced in the Appendix of SCHAEFFER (1992)

We say that the material is loading if $\partial_t(\sigma + \alpha\tau) > 0$, otherwise the material is unloading. We also say that the deformation is plastic if $\partial_t\gamma > 0$, and elastic otherwise.

This model has several important properties (GARAIZAR, 1993): *a*) the system of equations which describes the deformation is different for an elastic or plastic deformation, *b*) the system does not admit non-linear shocks (the only plastic waves are rarefactions-see 2.2) and *c*) the system loses hyperbolicity when γ reaches a critical value γ_c given by $H'(\gamma_c) = \alpha^{-2}$. Property *c*) relates to the formation of shear bands, the fundamental phenomenon studied in this paper; we explain some of its consequences in Section 3.

2.2 Wave curves

In this subsection we describe the variation of the state variables across hyperbolic waves, referring to GARAIZAR (1993) for some details. For a continuous solution, system (1) is equivalent to

$$\begin{pmatrix} 1 & 0 & 0 \\ 0 & 1+k & \alpha k \\ 0 & -\alpha k & 1-\alpha^2 k \end{pmatrix} \begin{pmatrix} v \\ \sigma \\ \tau \end{pmatrix}_t = \begin{pmatrix} 0 & c^2 & 0 \\ 1 & 0 & 0 \\ 0 & 0 & 0 \end{pmatrix} \begin{pmatrix} v \\ \sigma \\ \tau \end{pmatrix}_x \quad (3)$$

where

$$k(\gamma) = \begin{cases} H'(\gamma) & \text{if plastic loading} \\ 0 & \text{otherwise.} \end{cases} \quad (4)$$

The yield stress (2) evolves according to

$$\gamma(x, t) = \max_s \{ \sigma(x, s) + \alpha\tau(x, s) : s \leq t \}.$$

The eigenvalues associated to system (3) are those values of λ for which the matrix $\lambda A - D$ has zero determinant, where

$$A = \begin{pmatrix} 1 & 0 & 0 \\ 0 & 1+k & \alpha k \\ 0 & -\alpha k & 1-\alpha^2 k \end{pmatrix} \quad \text{and} \quad D = \begin{pmatrix} 0 & c^2 & 0 \\ 1 & 0 & 0 \\ 0 & 0 & 0 \end{pmatrix}.$$

An easy algebraic calculation shows that these eigenvalues are $\lambda = 0$ and $\lambda = \pm c\sqrt{\eta}$ with

$$\eta = \frac{1 - k\alpha^2}{1 + (1 - \alpha^2)k}. \quad (5)$$

These eigenvalues are real and distinct, and hence system (1) is hyperbolic, if and only if $\eta > 0$. We assume that $\alpha^2 < 1$ since the degree of nonassociativity is

typically small; moreover k is a nonnegative quantity. Thus from (5), system (1) is hyperbolic if and only if $k(\gamma) < \alpha^{-2}$, as claimed in point *c*) above.

For the zero eigenvalue: As we showed in GARAIJAR (1993), while the system is hyperbolic, the wave curves associated to $\lambda = 0$ are contact discontinuities which satisfy $[u] = [\sigma] = 0$ with $[\tau]$ and $[\gamma]$ as free parameters. Here $[a]$ represents the jump of the variable a across the corresponding wave; i.e., $[a] = a_r - a_l$, where a_r is the value of a to the right of the wave and a_l is the value to the left of the wave.

For the non-zero eigenvalues: The waves associated to $\lambda = \pm c\sqrt{\eta}$ can be either elastic or plastic. The elastic waves are linearly degenerate and satisfy $[\tau] = [\gamma] = 0$ and $[u] = -\lambda[\sigma]$ with wave speed $\lambda = (+/-)c$, for the left/right moving waves. The plastic waves are non-linear rarefactions with wave speeds $\lambda = (-/+)c\sqrt{\eta}$ and corresponding eigenvectors

$$R = \begin{pmatrix} c\sqrt{\eta} \\ (+/-)\eta \\ (+/-)\eta \frac{\alpha k}{1 - \alpha^2 k} \end{pmatrix}.$$

In the state space, the rarefaction curves are integral curves of the vector field given by the eigenvector R . We wish to parameterize these curves in terms of one of the state variables. For the most part we use σ as the parameter since σ is nonconstant on both elastic and plastic waves (by contrast, τ and γ are constant on elastic waves). However, for plastic waves with γ close to γ_c , the equation

$$\frac{d}{d\sigma} \begin{pmatrix} v \\ \tau \\ \gamma \end{pmatrix} = \begin{pmatrix} (+/-)c/\sqrt{\eta} \\ \alpha k/(1 - \alpha^2 k) \\ 1/(1 - \alpha^2 k) \end{pmatrix} \quad (6)$$

becomes singular as $k(\gamma) \rightarrow \alpha^{-2}$. For these waves we choose γ as the parameter. With this parameterization the rarefaction waves are described as the trajectories of the system of ordinary differential equations

$$\frac{d}{d\gamma} \begin{pmatrix} v \\ \sigma \\ \tau \end{pmatrix} = \begin{pmatrix} (+/-)c\sqrt{(1 - \alpha^2 k)(1 + (1 - \alpha^2)k)} \\ 1 - \alpha^2 k \\ \alpha^2 k \end{pmatrix}, \quad (7)$$

or, in terms of jumps of the state variables,

$$\begin{aligned} [v] &= (+/-)c \int_{\gamma_0}^{\gamma} \sqrt{(1 - \alpha^2 k(z))(1 + (1 - \alpha^2)k(z))} dz \\ [\sigma] &= [\gamma - \alpha^2 H(\gamma)] \\ [\tau] &= \alpha[H(\gamma)]. \end{aligned} \quad (8)$$

3 Solutions with shear bands

3.1 Jump conditions at the shear band

The loss of hyperbolicity for (1) is associated with the formation of shear bands. As in SCHAEFFER (1992), we idealize a shear band as a stationary point of discontinuity in a weak solution of (1). Although σ is continuous across a shear band, the other unknown functions can jump in crossing the shear band, and moreover at the point of discontinuity itself the stress variables τ and γ may assume values τ_b and γ_b different from either of the one sided limits (σ_b equals the common value of the one sided limits of σ). These variables "inside" the band are related to the variables outside the band by

$$\begin{aligned} \partial_t(\sigma_b + H(\gamma_b)) &= [v]/\delta \\ \partial_t(\tau_b - \alpha H(\gamma_b)) &= 0 \end{aligned} \tag{9}$$

where $[v] = v_{br} - v_{bl}$ is the jump in the velocity across the shear band (v_{bl} , v_{br} are the velocities at the left and right boundaries of the shear band) and δ is a "grain diameter" parameter discussed below. The evolution of the yield stress γ is, as in the hyperbolic case,

$$\gamma_b(x, t) = \max_s \{ \sigma_b(x, s) + \alpha \tau_b(x, s) : s \leq t \}.$$

These equations are supplemented by the two relations implicit in the above discussion; i.e.

$$s = 0 \quad \text{and} \quad [\sigma] = 0$$

where s denotes the speed of the point of discontinuity. These jump conditions play the role of the Rankine-Hugoniot conditions in gas dynamics. However, note that the jump conditions (9) include derivatives, not merely undifferentiated quantities as in the Rankine-Hugoniot conditions.

Let us briefly recall from SCHAEFFER (1992) the motivation for these jump conditions. A shear band in granular materials typically has a physical thickness, corresponding to the parameter δ above, of the order of ten grain diameters. Implicitly we are assuming that at a shear band the discontinuity has a "shock structure" as illustrated in Figure 1. The salient points of the figure are:

- (i) The velocity gradient is approximated by an average jump $\partial_x v = [v]/\delta$.
- (ii) The normal stress, σ , is constant throughout the shear band.
- (iii) The transversal stress, τ , jumps inside the band to a constant value which is larger than the one sided limits from the outside.

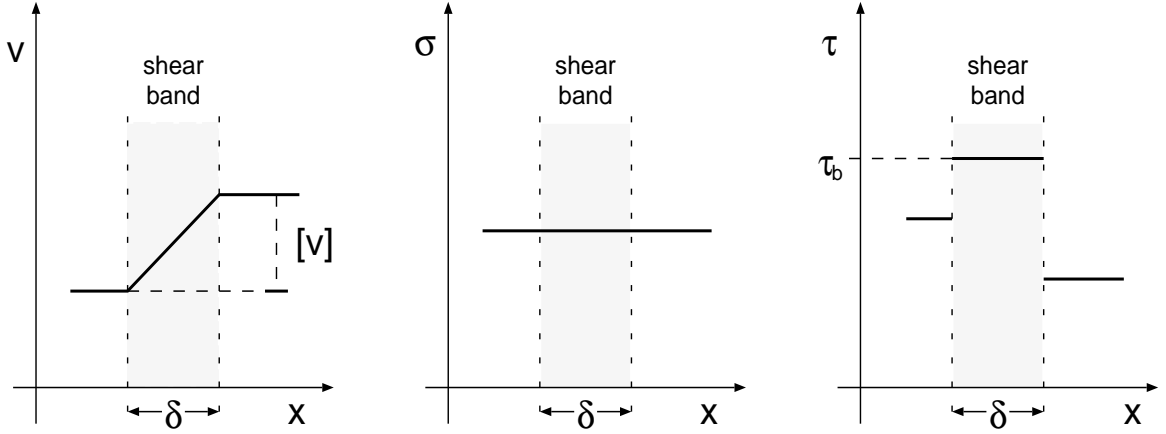


Figure 1: Structure of shear band.

Note that equations (9) are the same constitutive relations as in (1) except that the strain rate $\partial_x v$ has been replaced by $[v]/\delta$. In other words, the model assumes that when hyperbolicity is lost, the same constitutive behavior exists inside the shear band.

To elaborate on these issues, let us solve the last two equations in (3) for $\partial_t \sigma$:

$$\partial_t \sigma = \frac{1 - k\alpha^2}{1 + (1 - \alpha^2)k} \partial_x v. \quad (10)$$

Hyperbolicity is lost when $k = \alpha^{-2}$, so by (10) we have $\partial_t \sigma = 0$; i.e., the necessary condition for an extremum (in time). Moreover it is readily checked that, say for uniform loading (i.e., $\partial_x v = \text{const}$), we have $\partial_{tt} \sigma < 0$. In other words σ experiences a local maximum. Consequently, when a shear band forms and the material continues to load plastically inside it, σ_b decreases, so it is possible for σ_b to match up continuously with σ from unloading material outside the band. In Section 3.2 we consider an analytical solution with this behavior, and in Section 5, we exhibit numerical solutions with this behavior. For later reference it is convenient to solve (9) for the time derivatives of σ_b , τ_b and γ_b . If the shear band is loading plastically, we may deduce from (9) that

$$\frac{\partial}{\partial t} \begin{pmatrix} \sigma_b \\ \tau_b \\ \gamma_b \end{pmatrix} = \begin{pmatrix} 1 - \alpha^2 H'(\gamma_b) \\ \alpha H'(\gamma_b) \\ 1 \end{pmatrix} \frac{1}{1 + (1 - \alpha^2) H'(\gamma_b)} \frac{v_{br} - v_{bl}}{\delta}. \quad (11)$$

If the shear band is deforming elastically we have

$$\frac{\partial}{\partial t} \begin{pmatrix} \sigma_b \\ \tau \\ \gamma_b \end{pmatrix} = \begin{pmatrix} 1 \\ 0 \\ 0 \end{pmatrix} \frac{v_{br} - v_{bl}}{\delta}. \quad (12)$$

In concluding we remark explicitly that a shear band represents a tear in the material - the displacement, not merely the velocity, is discontinuous.

3.2 Riemann problem with a shear band

A Riemann problem is an initial value problem with initial data consisting of two constant states:

$$U(x, 0) = \begin{cases} U_L, & x < 0 \\ U_R, & x > 0. \end{cases}$$

In this section we describe the structure of the solution to a Riemann problem which does not admit a selfsimilar solution. We start with a description of the states U connected to a given state $U_0 = (v_0, \sigma_0, \tau_0, \gamma_0)^t$ by a right or left moving wave. First we define the auxiliary function

$$\phi(\sigma, U_0) = c \int_{\sigma_0}^{\sigma} [\eta(\gamma(\xi))]^{-1/2} d\xi$$

where γ , as a function of σ , is given by $\gamma(\sigma) = \gamma_0$ if $\sigma < \gamma_0 - \alpha\tau_0$ (U is in the elastic region) and by the solution to equation (8b),

$$\sigma = \gamma - \alpha\tau_0 - \alpha^2(H(\gamma) - H(\gamma_0)),$$

otherwise (U is in the plastic region). In both cases $\tau(\sigma) = \tau_0 + \alpha(H(\gamma(\sigma)) - H(\gamma_0))$. With this notation we write $W_{\mp}(\sigma, U_0)$, the solutions to equation (6), as

$$W_-(\sigma, U_0) = \begin{pmatrix} v_0 + \phi(\sigma, U_0) \\ \tau(\sigma) \\ \gamma(\sigma) \end{pmatrix}$$

(the one parameter family of states connected to U_0 by a left moving wave) and

$$W_+(\sigma, U_0) = \begin{pmatrix} v_0 - \phi(\sigma, U_0) \\ \tau(\sigma) \\ \gamma(\sigma) \end{pmatrix}$$

(the one parameter family of states connected to U_0 by a right moving wave).

We notice that $d\phi/d\sigma \geq 0$ for the states in the hyperbolic region. Therefore the projections on the $\sigma - v$ plane of the wave curves $W_{\mp}(\sigma, U_0)$ are monotone in that region.

Given the initial left and right states U_L and U_R , the Riemann problem admits a traditional (selfsimilar) solution $U(x, t) = \hat{U}(x/t)$ if the curves $W_-(\sigma, U_L)$ and $W_+(\sigma, U_R)$ intersect on the $\sigma - v$ plane (see Figure 2a).

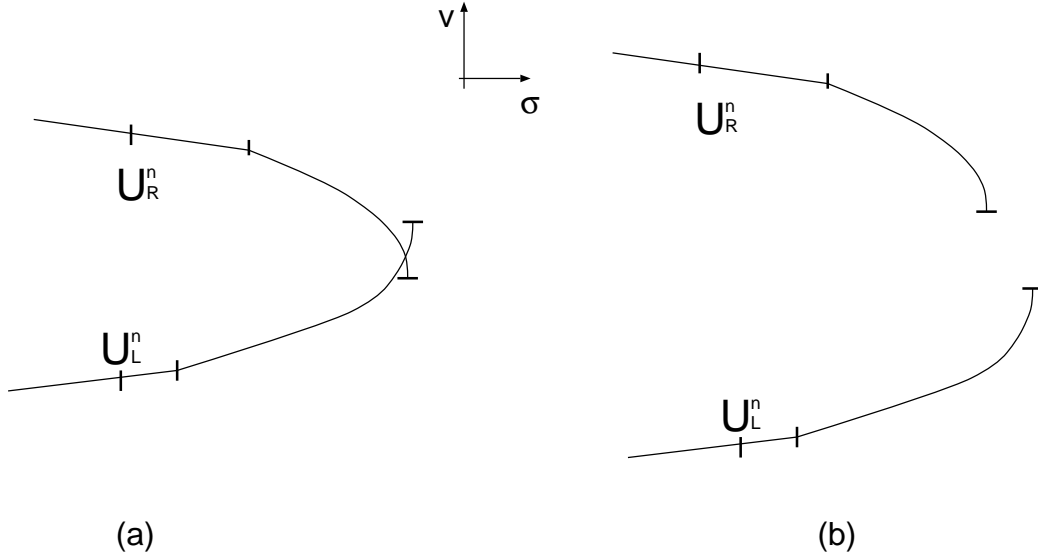


Figure 2: Wave curves for a traditional and nontraditional Riemann problem.

As shown in GARAIZAR (1993), the the projections of the wave curves are bounded as σ approaches its maximum value (i.e.; $\gamma \rightarrow \gamma_c$). This means that although the Riemann problem is solvable for initial states which are close, if the difference between the initial states is large enough, the wave curves $W_-(\sigma, U_L)$ and $W_+(\sigma, U_R)$ do not intersect in the $\sigma - v$ plane for states in the hyperbolic region (see Figure 2b).

The resolution of Riemann problems is fundamental in algorithms of Godunov type and Front-tracking methods. While tracking a hyperbolic front, the position of the updated front is given by the solution to a Riemann problem. In our case, the front we need to track, a shear band, is non-hyperbolic and static; i.e, the front does not change position once it is formed. Nevertheless, we need to solve the non-traditional Riemann problem, where selfsimilarity fails (see Figure 2b), in order to originate the front.

SHEARER and SCHAEFFER (1993) give a description of the local existence of solutions to such a problem (see Figure 3 and note that loading occurs only in shaded region). This solution consists of two packs of hyperbolic waves (elastic precursor followed by plastic rarefactions) connected in the $x - t$ plane by a shear band and

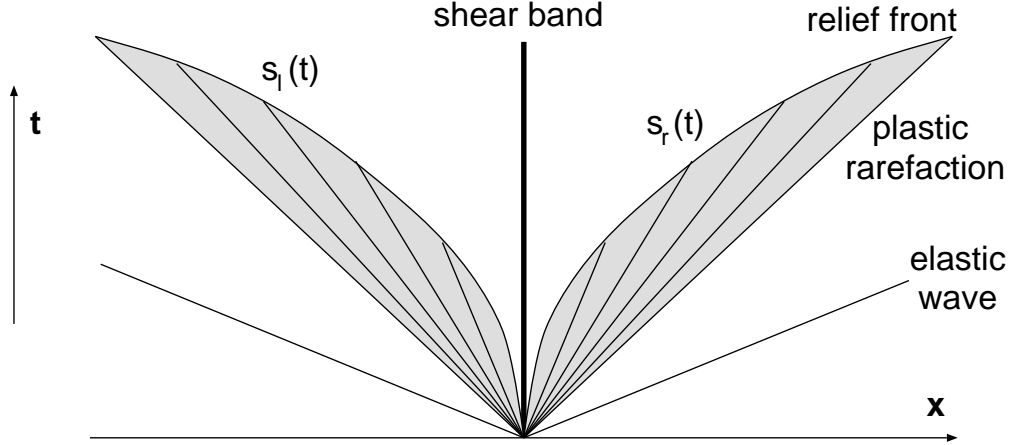


Figure 3: Shear band formation.

two regions of elastic unloading. The boundary between these elastic regions and the hyperbolic waves is called a relief front. These fronts originate at the point of formation of the shear band and travel at increasing speed as they interact with the plastic rarefactions. We now proceed to describe the solution near the shear band. As in SHEARER and SCHAEFFER (1993), we express the Riemann problem as a coupled free boundary problem with equations

$$\begin{aligned}\partial_t v &= c^2 \partial_x \sigma \\ \partial_t \sigma &= \partial_x v\end{aligned}\tag{13}$$

in the planar domains $\{(x, t) : t > 0, 0 < x < s_r(t)\}$, and $\{(x, t) : t > 0, 0 > x > s_l(t)\}$ where the relief fronts $x = s_l(t)$ and $x = s_r(t)$ are to be determined. These fronts separate the plastic rarefaction from the region where the material goes into unloading.

At the free boundaries, the system is subject to the boundary conditions

$$\begin{aligned}\sigma(s_l(t), t) &= \hat{\sigma}(s_l(t)/t), \\ v(s_l(t), t) &= \hat{v}(s_l(t)/t), \\ \sigma(s_r(t), t) &= \hat{\sigma}(s_r(t)/t), \\ v(s_r(t), t) &= \hat{v}(s_r(t)/t).\end{aligned}\tag{14}$$

Here, $\hat{\sigma}$ and \hat{v} are the components of the selfsimilar solution to system (1)(2) in the domains $\{(x, t) : t > 0, s_l(t) > x\}$ and $\{(x, t) : t > 0, s_r(t) < x\}$.

We introduce the notation $\sigma_b(t) = \sigma(0, t)$, $\gamma_b(t) = \gamma(0, t)$ and $\tau_b(t) = \tau(0, t)$ for the stress components at the shear band and $v_{bl}(t) = v(0-, t)$ and $v_{br}(t) = v(0+, t)$

for the velocity component of the solution at the left and right edges of the shear band for $t > 0$. At the shear band, $x = 0$, the system is subject to a nonlinear boundary condition given by (11) (Notice that for the Riemann problem, the shear band is in plastic loading for all $t > 0$.)

Therefore, the solution to our initial value problem satisfies a linear system (13) on $\{t > 0, 0 > x > s_l(t)\}$ and $\{t > 0, 0 < x < s_r(t)\}$ with nonlinear boundary conditions (14)(11), a nonlinear system (1)(2) on $\{t > 0, s_l(t) > x\}$ and $\{t > 0, s_r(t) < x\}$, and is continuous at $x = s_l(t)$ and $x = s_r(t)$ where the functions $s_l(t)$ and $s_r(t)$ are to be determined.

As we mention above, the local existence of solutions to this problem is proved in SHEARER and SCHAEFFER (1993) for the symmetric case ($v_l = -v_r$, $\sigma_l = \sigma_r$, $\tau_l = \tau_r$ and $\gamma_l = \gamma_r$). In Appendix B we give a proof for the global existence for this case. In Appendix A we describe a numerical implementation for the solution of this Riemann problem (determining the states at the shear band and the position of the relief fronts.) This method will be used as a comparison for the solutions obtained by the numerical algorithm described next.

4 Numerical Algorithms

For the numerical resolution of the shear band we will adapt ideas from front tracking methods; specifically the flux redistribution techniques of CHERN and COLELLA (1987). We should notice that the problem we are about to describe is not exactly a front tracking problem in the sense that the shear band is not a hyperbolic wave; rather it is treated as an static internal boundary.

On cells where the original system (1) is still hyperbolic, we will use a hyperbolic scheme like that described in GARAIZAR (1993) or an adaptation of a Godunov-characteristic tracing method like that of TRANGENSTEIN and PEMBER (1992). On cells which are close to a shear band, we switch to a first order Godunov method. This is done to avoid spurious formation of shear bands due to the linear reconstruction of the states on the cell. At the shear band itself, we use a numerical implementation of (9).

4.1 Calculation before the formation of the shear band

We divide the spatial domain into N cells of size Δx_j and centered at the point x_j for $1 \leq j \leq N$. We denote by $x_{j+\frac{1}{2}}$ the location of the right boundary for the j^{th} cell; $x_{j+\frac{1}{2}} = x_j + \Delta x_j/2$. We write U_j^n for the average of the state over the j^{th} cell at time $t = t_n$. We assume that for a given n , the cell averages U_j^n are known for $1 \leq j \leq N$.

We describe an algorithm to compute U_j^{n+1} , the cell averages at time $t = t_n + \Delta t$, where Δt is the time increment.

The state U at a given cell has four components: u , σ , τ and γ , and therefore we need four equations to describe the updating of the state averages. The first three equations are provided by the conservative system (1)

$$G(U)_t + F(U)_x = 0, \quad (15)$$

where $G(U) = \begin{pmatrix} u \\ \sigma + H(\gamma) \\ \tau - \alpha H(\gamma) \end{pmatrix}$ and $F(U) = \begin{pmatrix} -c^2 \sigma \\ -u \\ 0 \end{pmatrix}$. Discretization of these equations yields

$$G(U_j^{n+1}) = G(U_j^n) - \frac{\Delta t}{\Delta x_j} \left(F_{j+\frac{1}{2}}^{n+\frac{1}{2}} - F_{j-\frac{1}{2}}^{n+\frac{1}{2}} \right) \quad (16)$$

where $F_{m+\frac{1}{2}}^{n+\frac{1}{2}} = F(U_m^n, U_{m+1}^n)$ is the numerical flux evaluated at the state on the cell edge given by $x_{m+\frac{1}{2}}$. This flux is calculated as the solution to an exact or linearized Riemann Problem (GARAIZAR, 1993) with initial states chosen appropriately as to generate a first or second order hyperbolic scheme.

A fourth equation is needed to complete the description of the algorithm. For this equation we need to know if the material behavior is elastic or plastic. We write the two nonzero components of the numerical flux in (16) as

$$\begin{aligned} f_v &= c^2 (\sigma_{j+\frac{1}{2}}^{n+\frac{1}{2}} - \sigma_{j-\frac{1}{2}}^{n+\frac{1}{2}}) \Delta t / \Delta x_j \\ f_\sigma &= (v_{j+\frac{1}{2}}^{n+\frac{1}{2}} - v_{j-\frac{1}{2}}^{n+\frac{1}{2}}) \Delta t / \Delta x_j. \end{aligned} \quad (17)$$

If f_σ does not exceed the gap between the current yield γ_j^n and the current total stress $\sigma_j^n + \alpha \tau_j^n$; i.e., if

$$f_\sigma \leq \gamma_j^n - (\sigma_j^n + \alpha \tau_j^n), \quad (18)$$

the states on the j^{th} cell at the time t , $n\Delta t \leq t \leq (n+1)\Delta t$, will be elastic. Therefore we can complete (16) by

$$\begin{aligned} v_j^{n+1} &= v_j^n + f_v, \\ \sigma_j^{n+1} &= \sigma_j^n + f_\sigma, \\ \tau_j^{n+1} &= \tau_j^n, \\ \gamma_j^{n+1} &= \gamma_j^n, \end{aligned} \quad (19)$$

where we have written out the components of (16) as well as included the fourth equation. On the other hand, if the numerical flux exceeds the gap between the current yield and the current total stress ($f_\sigma \geq \gamma_j^n - (\sigma_j^n + \alpha \tau_j^n)$), the deformation will turn plastic during this time step. In this case we define $\sigma_{max} = \gamma_j^n - \alpha \tau_j^n$, as

the maximum value to which σ can be increased with the state remaining elastic. We define the plastic flux $f_p = f_\sigma - (\sigma_{max} - \sigma_j^n)$ or the difference between the numerical stress flux f_σ and the gap between the current yield and the current total stress. We now write (16) as

$$\begin{aligned} v_j^{n+1} &= v_j^n + f_v, \\ \sigma_j^{n+1} + H(\gamma_j^{n+1}) &= \sigma_j^n + H(\gamma_j^n) + f_\sigma = \sigma_{max} + H(\gamma_j^n) + f_p, \\ \tau_j^{n+1} - \alpha H(\gamma_j^{n+1}) &= \tau_j^n - \alpha H(\gamma_j^n), \\ \gamma_j^{n+1} &= \sigma_j^{n+1} + \alpha \tau_j^{n+1}. \end{aligned} \tag{20}$$

We note that (20) can be reduced to a single implicit equation for γ_j^{n+1}

$$\Sigma(\gamma_j^{n+1}) = \Sigma(\gamma_j^n) + f_p \tag{21}$$

where $\Sigma(\gamma) = \gamma + (1 - \alpha^2)H(\gamma)$ is a monotone function ($\Sigma'(\gamma) = 1 + (1 - \alpha^2)H'(\gamma) > 0$). This observation makes equation (21) easy to solve.

After each hyperbolic sweep we inspect the updated states U_j^{n+1} for states outside the hyperbolic region (i.e., $H(\gamma_j^{n+1}) > \alpha^{-2}$). If the state $U_{j_b}^{n+1}$ at some j_b^{th} cell is not in the hyperbolic region, we proceed to the creation of a shear band in that cell.

4.2 Initialization of the shear band

When the system loses hyperbolicity, the previous algorithm must be modified. This loss of hyperbolicity can occur in two ways:

- (a) A new state U_j^{n+1} is not hyperbolic ($H(\gamma_j^{n+1}) > \alpha^{-2}$) or
- (b) a Riemann Problem at a cell edge does not admit a classical self-similar solution.

We discuss the first case in detail; the second case will easily follow from the first one. To be specific, suppose that at time $t_n + \Delta t$ the state $U_{j_b}^{n+1}$, in a given cell j_b , is not hyperbolic for the first time. In order to make the following exposition simpler, we will assume that states for two contiguous cells do not leave the hyperbolic region simultaneously (Figure 4). (Even though we do not discuss it here, our algorithm can deal with the simultaneous formation of a shear band in a small number of contiguous cells.) The initialization process proceeds by (i) putting a shear band at a point in the j_b^{th} cell, (ii) expanding the data structure to accommodate the shear band (introducing the states U_b at the band and U_l and U_r next to the band, see Figure 4) and (iii) recomputing the evolution of the solution at the n^{th} time step for the states affected by the shear band: $U_{j_b-1}^{n+1}$, U_l^{n+1} , U_b^{n+1} , U_r^{n+1} and $U_{j_b+1}^{n+1}$. Let us discuss these steps in sequence.

(i) **Localization in space.** We compare the states $U_{j_b-1}^{n+1}$, $U_{j_b}^{n+1}$ and $U_{j_b+1}^{n+1}$. For x_j , the midpoint of the j^{th} -cell, we will fit the points $(x_{j_b-1}, \gamma_{j_b-1}^{n+1})$, $(x_{j_b}, \gamma_{j_b}^{n+1})$ and $(x_{j_b+1}, \gamma_{j_b+1}^{n+1})$ by a parabola. Since $\gamma_{j_b}^{n+1} > \gamma_{j_b\pm 1}^{n+1}$, the maximum (x_b, γ_b) of the parabola will satisfy $x_b \in (x_{j_b-\frac{1}{2}}, x_{j_b+\frac{1}{2}})$. We place the shear band at $x = x_b$. For future reference we define the size of the subcells next to shear band by $d_l = x_b - x_{j_b-\frac{1}{2}}$ and $d_r = \Delta x_{j_b} - d_l$.

When a shear band is formed as result of a non-self similar solution to a Riemann Problem at a cell boundary $x_{j_b+\frac{1}{2}}$ (case (b) above), we localize the band in the j_b^{th} cell with $d_l = \Delta x_{j_b}$ and $d_r = 0$.

(ii) **Origination of the states associated to the shear band.** In addition to x_b , d_l and d_r , the cell containing the shear band needs further data as follows (see Figure 4): The average states on the subcells, U_l and U_r , and the stress components of the state on the band, U_b . (No velocity is specified on the shear band -see Figure 1.)

We initialize the states U_l^n and U_r^n with convex combinations of the neighboring states; in symbols

$$U_l^n = (d_l U_{j_b}^n + (\Delta x_{j_b} - d_l) U_{j_b-1}^n) / \Delta x_{j_b}$$

$$U_r^n = (d_r U_{j_b}^n + (\Delta x_{j_b} - d_r) U_{j_b+1}^n) / \Delta x_{j_b}$$

The components of U_b^n (σ_b^n , τ_b^n and γ_b^n) are initialized as the solution (on the shear band at the time of formation of the band) of the extended Riemann Problem SHEARER and SCHAEFFER (1993) with initial states U_l^n and U_r^n (see Section 3.2).

(iii) **Evolution of the states associated to the shear band** The integration along the shear band and modification of the contiguous states is carried out as described for a regular step in the next section.

4.3 Modification of the integration algorithm near the shear band

We now describe the algorithm for updating the solution on a cell containing the shear band and modifying the updated states on neighboring cells. We should note that this algorithm is not fully conservative. Although all three equations in (1) are in conservation form, across the shear band, only momentum is conserved. This is reflected in our algorithm, where the numerical flux related to the momentum equation will be conserved across the computational domain, but not the numerical flux associated to the constitutive equations.

As above let j_b denote the index of the cell containing the shear band. We assume that at time t_n , the states $U_{j_b-1}^n$, $U_{j_b+1}^n$, U_l^n , U_r^n and U_b^n are known and we must

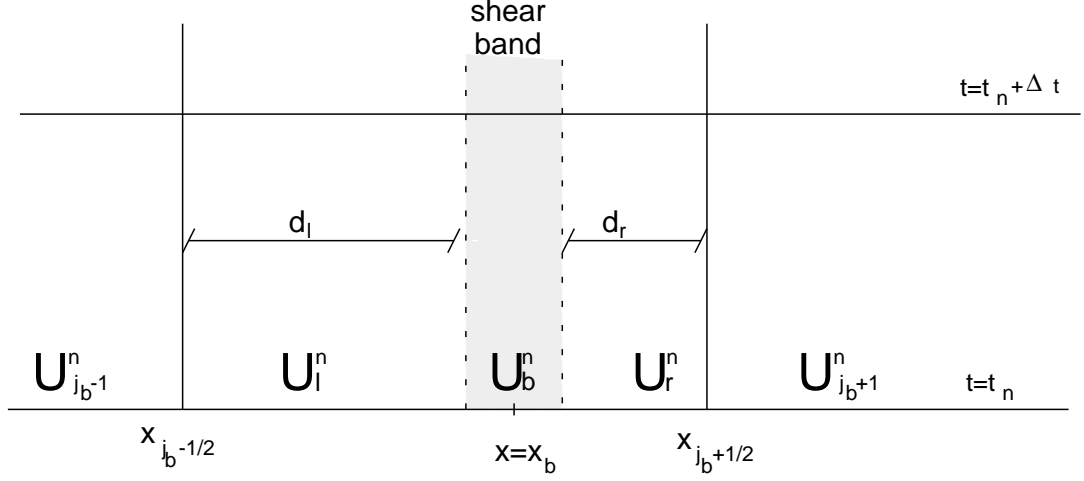


Figure 4: Initialization of the shear band.

find the states $U_{j_b-1}^{n+1}$, $U_{j_b+1}^{n+1}$, U_l^{n+1} , U_r^{n+1} and U_b^{n+1} at time $t_n + \Delta t$. The algorithm is performed in 2 steps:

- (i) advance the state inside the shear band, U_b^{n+1} , and
- (ii) advance the states U_l^{n+1} and U_r^{n+1} next to the shear band and correct the states $U_{j_b-1}^{n+1}$, $U_{j_b+1}^{n+1}$.

(i) **Advance the state on the shear band.** U_b^{n+1} . We obtain U_b^{n+1} by integrating (9), or its elastic (12), and plastic (11) versions, from t_n to $t_n + \Delta t$. Since the hyperbolic scheme near the shear band is of first order, the integration of the band is done also with first order accuracy. For that reason we may consider the right hand side of equation (9) to be constant. We now explain how we determine this constant value. First, since the state U_l^n could be unreliable for small values of d_l , we replace U_l^n by U_L^n , a convex linear combination of $U_{j_b-1}^n$ and U_l^n with weights $(\Delta x_{j_b} - d_l)/\Delta x_{j_b}$ and $d_l/\Delta x_{j_b}$. Similarly we calculate U_R^n to replace U_r^n :

$$U_L^n = \frac{\Delta x_{j_b} - d_l}{\Delta x_{j_b}} U_{j_b-1}^n + \frac{d_l}{\Delta x_{j_b}} U_l^n$$

$$U_R^n = \frac{\Delta x_{j_b} - d_r}{\Delta x_{j_b}} U_{j_b+1}^n + \frac{d_r}{\Delta x_{j_b}} U_r^n$$

We then obtain U_{bl}^n , the state on the left boundary of the shear band at time t_n , as the state connected to U_L^n by left moving waves and with the normal stress given by

the state on the shear band, $\sigma_{bl}^n = \sigma_b^n$ (see Figure 5). A similar process defines U_{br}^n . Finally we assign the constant value to the velocity jump $v_{br} - v_{bl} = v_{br}^n - v_{bl}^n$ for $t_n \leq t < t_n + \Delta t$, where v_{bl}^n and v_{br}^n are the velocity components of the states U_{bl}^n and U_{br}^n .

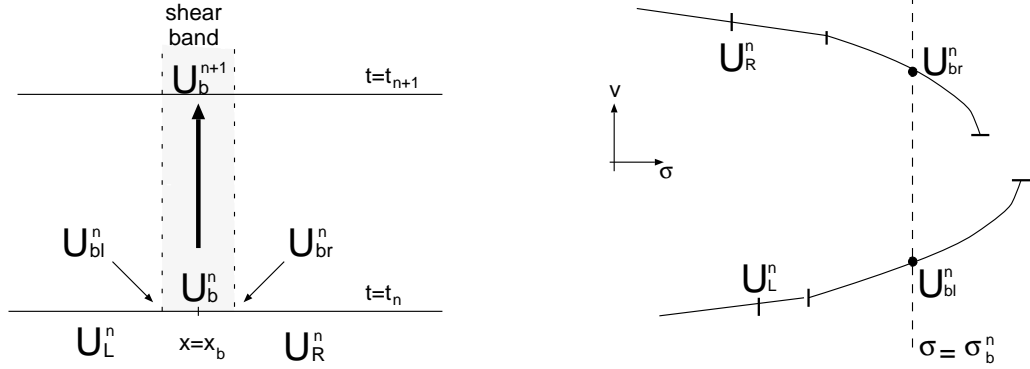


Figure 5: Shear band Integration.

(ii) **Advance the neighboring states on the shear band.** $U_l^{n+1}, U_r^{n+1}, U_{j_b-1}^{n+1}, U_{j_b+1}^{n+1}$

We describe the corrections to the updated states $U_{j_b \pm 1}^{n+1}$ as well as the updating of the states U_l^{n+1} and U_r^{n+1} next to the shear band. We will explain in detail how it is done for the states on the left. The right states are updated similarly.

The conservative finite differences algorithm for the cell $j_b - 1$ was given by

$$G(U_{j_b-1}^{n+1}) = G(U_{j_b-1}^n) + \frac{\Delta t}{\Delta x_{j_b-1}} (F_{j_b-3/2}^{n+1/2} - F_{j_b-1/2}^{n+1/2}) \quad (22)$$

Three corrections need to be made to the algorithm:

- As was explained above, we replace U_l^n by U_L^n .
- The flux $F_{j_b-1/2}^{n+1/2}$ needs to be corrected in order to account for the shear band (Figure 6). We define $\hat{F}_{j_b-1/2}^{n+1/2} = F(U_{j_b-1}^n, U_L^n)$ as the corrected numerical flux on the left edge of the j_b^{th} cell and write

$$\Delta \hat{M}_{j_b-1}^{n+1/2} = \Delta t (F_{j_b-3/2}^{n+1/2} - \hat{F}_{j_b-1/2}^{n+1/2}), \quad (23)$$

which will be used to recalculate (22).

- A further correction to the algorithm is made to include the redistributed mass obtained from the integration on the subcell next to the band. The final expression for the algorithm on the j_b^{th} cell and the left subcell is:

$$G(U_{j_b-1}^{n+1}) = G(U_{j_b-1}^n) + \frac{\Delta \hat{M}_{j_b-1}^{n+1/2}}{\Delta x_{j_b-1}} + \frac{\Delta x_{j_b} - d_l}{\Delta x_{j_b}} \Delta M_l^{n+1/2} \quad (24)$$

$$G(U_i^{n+1}) = G(U_L^n) + \frac{\Delta M_l^{n+1/2}}{\Delta x_{j_b}} + \frac{\Delta x_{j_b} - d_l}{\Delta x_{j_b}} \Delta M_l^{n+1/2} \quad (25)$$

We now derive these formulas.

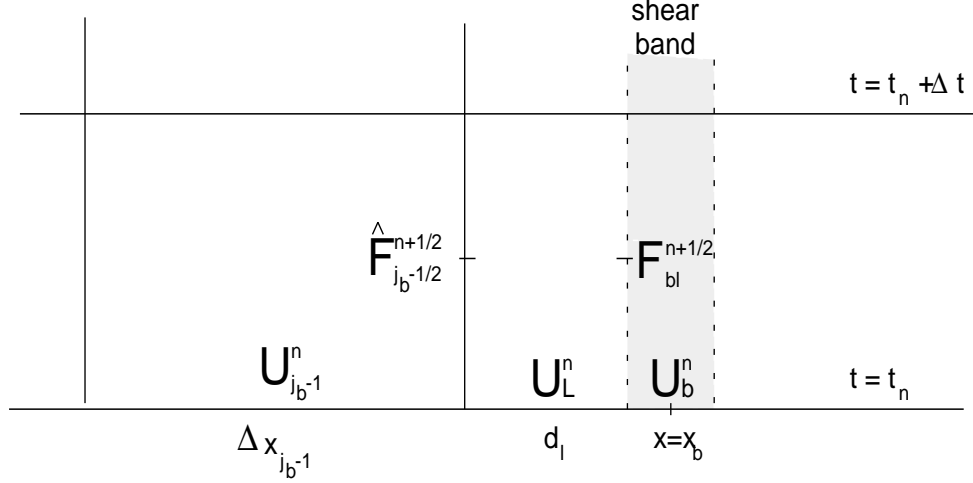


Figure 6: Flux modifications on left of band.

We write the flux for the subcell to the left of the shear band as

$$\Delta M_l^{n+1/2} = \Delta t (\hat{F}_{j_b-1/2}^{n+1/2} - F_{bl}^{n+1/2}) \quad (26)$$

where $F_{bl}^{n+1/2} = F(U_{bl}^{n+1/2})$ is the flux on the left boundary of the shear band at time $t_n + \Delta t/2$ (see Figure 6). $U_{bl}^{n+1/2}$ is obtained as in part (i) but, this time, with right boundary condition $\sigma = (\sigma_b^n + \sigma_b^{n+1})/2$. The conservative algorithm on the left subcell would have been given by

$$G(U_i^{n+1}) = G(U_L^n) + \frac{\Delta M_l}{d_l}, \quad (27)$$

but, if d_l is too small equation (27) would violate the CFL condition $\frac{\Delta t}{\Delta x} \leq \text{const} < 1$. In the spirit of Chern-Colella's method (CHERN and COLELLA, 1987), we replace $\Delta M_l^{n+1/2}$ by $\Delta Q_l = \frac{d_l}{\Delta x_{j_b}} \Delta M_l^{n+1/2}$ and tentatively modify (27) to read

$$G(U_i^{n+1}) = G(U_L^n) + \frac{\Delta Q_l}{d_l} = G(U_L^n) + \frac{\Delta M_l^{n+1/2}}{\Delta x_{j_b}} \quad (28)$$

which gives a stable algorithm.

The final step is to put the residual flux $\Delta M_l^{n+1/2} - \Delta Q_l$ back in the system. We will distribute this residual flux over the $(j_b - 1)^{th}$ cell and the left subcell. We therefore write

$$\Delta x_{j_b-1} G(U_{j_b-1}^{n+1}) = \Delta x_{j_b-1} G(U_{j_b-1}^n) + \Delta M_{j_b-1}^{n+1/2} + \frac{\Delta x_{j_b-1}}{\Delta x_{j_b-1} + d_l} (\Delta M_l^{n+1/2} - \Delta Q_l) \quad (29)$$

$$d_l G(U_l^{n+1}) = d_l G(U_L^n) + \Delta Q_l + \frac{d_l}{\Delta x_{j_b-1} + d_l} (\Delta M_l^{n+1/2} - \Delta Q_l), \quad (30)$$

which on simplification gives (24) and (25).

5 Examples

In this section we show several numerical examples for the algorithm described in the previous section. The first example corresponds to the Riemann problem studied in Section 3.2. We use this example to validate the numerical method: the position of the relief front and the states inside the shear band that are determined numerically agree well with the analytical solution. (cf. Appendix A for a description of the numerical implementation for this analytical solution.) The other two examples correspond to deformations with uniform loading in a material with one or two defects. For these last examples we do not have an analytical solution; rather the numerical solution provides new information. Regarding the third example, the competition between two incipient shear bands is an interesting phenomenon deserving further study.

5.1 Riemann Data

In this subsection we obtain the numerical solution to a Riemann problem with formation of shear bands as studied in Section 3.2. We assume linear hardening of the material ($k(\gamma) = \frac{1}{(1-\gamma)}$ or $H(\gamma) = -\log(1-\gamma)$), nonassociativity parameter $\alpha = 0.35$, shear band width $\delta = 0.05$ and the elastic speed $c = 1$. For a material with these properties we consider initial states

- $(v, \sigma, \tau, \gamma) = (-.48, .56, 0, .61)$ for $x < 0$ and
- $(v, \sigma, \tau, \gamma) = (.48, .56, 0, .61)$ for $x > 0$.

The Riemann problem with these initial data does not support a classical selfsimilar solution (see Figure 7) and a shear band is formed at $x = 0$.

In Figure 7 we show the wave curves in the $\sigma - v$ plane. We observe the elastic precursor waves loading the material from $\sigma = .56$ to $\sigma = .61$ followed by the plastic rarefactions up to the point of material failure at $\sigma = .7356$, $\gamma = .8775$. The hyperbolic waves do not intersect in the $v - \sigma$ plane and therefore a classical

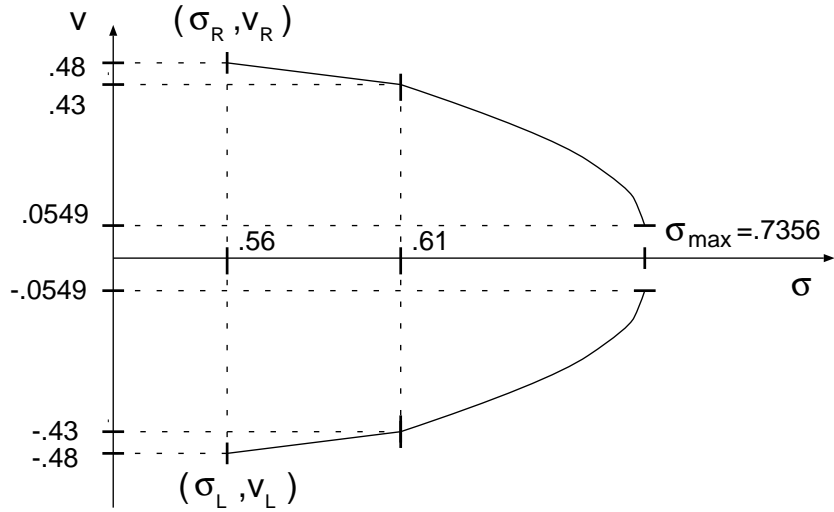


Figure 7: Riemann data and partial wave curves.

selfsimilar solution to this initial value problem does not exist. The solution exhibits symmetry about the line $x = 0$. This symmetry is observed in our calculations. In this example we reduce the spatial domain to a non-symmetric interval $-.5 < x < .025$ with non-reflective boundary conditions at $x = -.5$ and $x = .025$. We divide the spatial domain in cells of size $\Delta x = .0005$.

In Figure 8 we show the profiles of the velocity v and the normal stress σ at time $t = .35955$ compared to the initial data (dotted line). We clearly observe the full structure of the solution: the linear elastic wave and the plastic rarefaction followed by the relief front connecting to the shear band. (Note: We should notice that the velocity v is an odd function of x while the stresses σ , τ and γ are even.)

A material point is loading when γ increases with time, that is the trajectory crosses the γ level curves. In Figure 9 we show the level curves for the yield stress γ (dashed lines). For points in the $x-t$ plane where the level curves are slanted, the material is in an state of plastic loading; while for points in the $x-t$ plane where the level curves are vertical the corresponding deformations are elastic. The relief front corresponds to the points of transition from plastic to elastic deformations. Graphically this corresponds to points where the level curves turn vertical.

In Figure 9 we also superimpose the leading edge of the rarefaction (solid line) and the relief front obtained by the numerical bootstrap calculation described in Appendix A (dot-dashed line). We observe how the relief front travels faster than the rarefaction and absorbs the leading edge of the rarefaction at approximately $t = .86$. We notice that the "bootstrap" method is unrelated to the hyperbolic scheme described in the previous section and is a numerical equivalent to the analytical solution

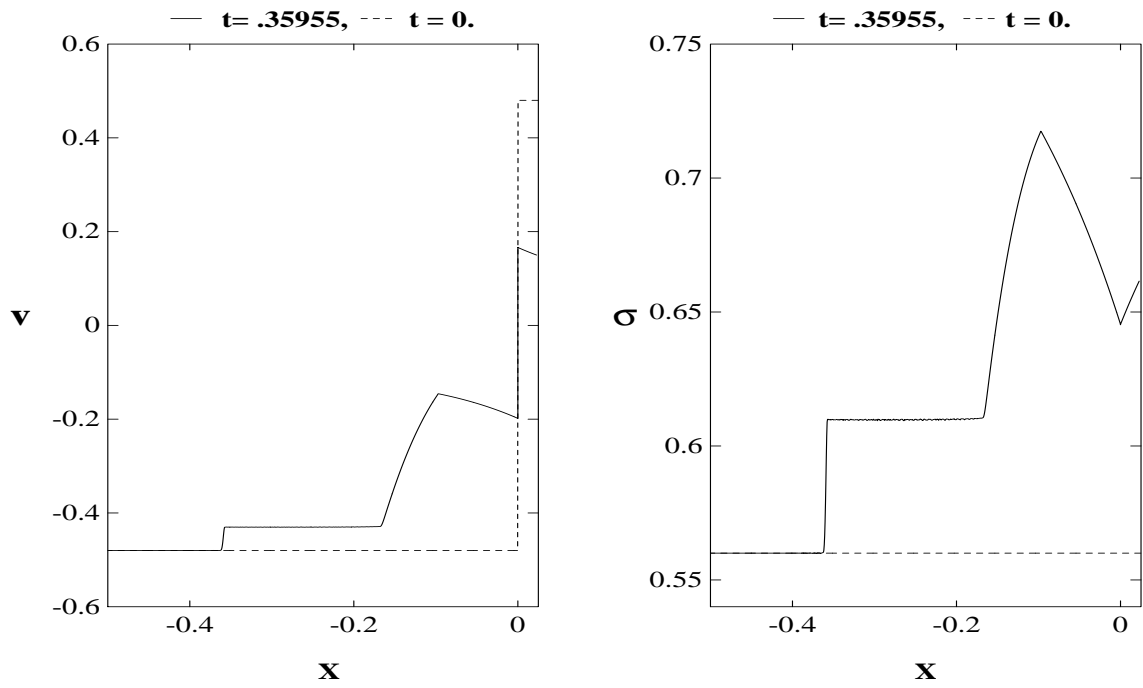


Figure 8: Stress and velocity.

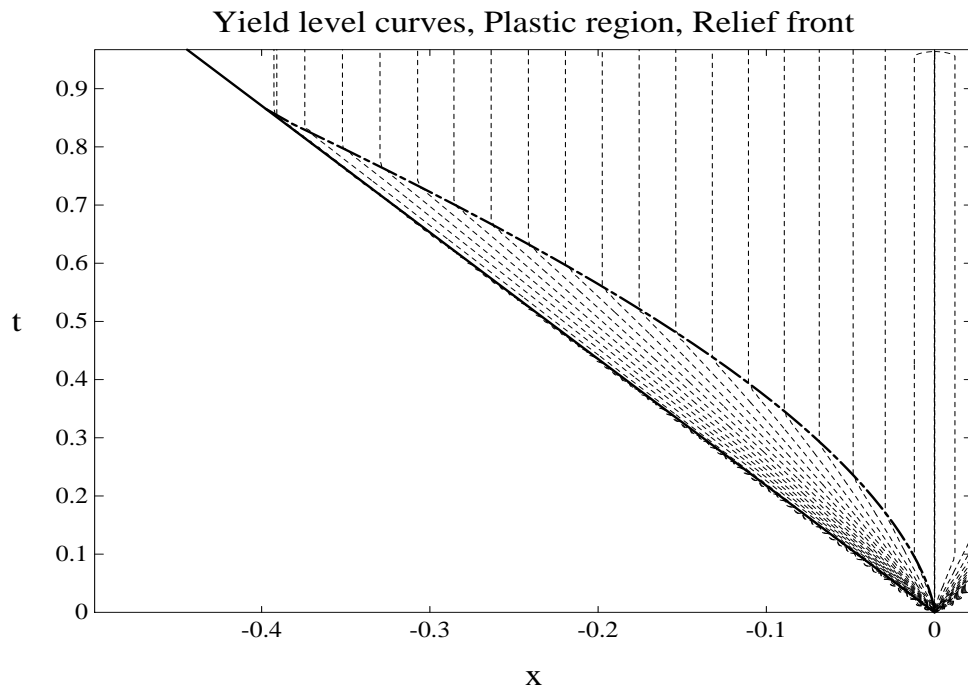


Figure 9: Yield stress level curves .

described in SHEARER and SCHAEFFER (1993). We observe the close agreement on the location of the relief front by both methods (dot-dashed = bootstrap, corners on level curves = hyperbolic scheme).

In Figure 10 we show γ , the yield stress, at time $t = .35955$ and $t = .8658$, when the relief front completely overtakes the rarefaction wave. In Figure 11 we compare the values of u at the left edge of the shear band and σ and γ at the shear band by both methods (solid = bootstrap, dotted = hyperbolic scheme).

In this initial paper, to capture small scale effects in the unloading region near the shear band, we used an exceedingly fine mesh. The mesh size was in fact less than the grain size parameter δ . This does not pose a theoretical difficulty since if the numerical method converges as the mesh parameter tends to zero, it does not matter how small this parameter is taken. However, it is unacceptable on practical grounds since using such a small mesh parameter would make calculations for realistic problems prohibitively expensive. We plan further work devoted to increasing the mesh size with two approaches using: (i) a uniformly larger grid size and (ii) an adaptively refined mesh with small cells only near the shear band.

5.2 Uniform loading with one defect

For the next example we consider a problem of uniform loading, as a one dimensional version of the problem proposed in Section 2b of SCHAEFFER (1992). In the domain $-.525 < x < .525$ we consider initial data where the stresses are constant ($\sigma(x, 0) = \sigma_0$, $\gamma(x, 0) = \gamma_0$ and $\tau(x, 0) = \tau_0$) and the velocity is linear ($v(x, 0) = \mu x$). At the boundary we keep the velocity constant. This type of initial data provides a uniform loading along the sample; i.e., for homogeneous materials, the solution satisfies that the stresses are constant in space ($\sigma(x, t) = \sigma(t)$, $\gamma(x, t) = \gamma(t)$ and $\tau(x, t) = \tau(t)$) and the velocity is constant in time ($v(x, t) = \mu x$). We introduce an inhomogeneity in the material at $x = 0$ which reduces the critical value of γ for which system (1)(2) loses hyperbolicity. We expect the sample to exhibit a shear band formation at $x = 0$, before it happens anywhere else in the sample.

We divide the spatial domain in cells of size $\Delta x = .005$. We impose initial data $\sigma(x, 0) = .7485$, $\gamma(x, 0) = .7485$, $\tau(x, 0) = 0$ and ($v(x, 0) = x/10$) with material parameters across the sample as in the previous example. We introduce an inhomogeneity at $x = 0$ by changing the value of α at this point to $\alpha = .5$. This will assure the formation of a shear band at $x = 0$ when $\gamma = .75$.

In Figure 12 we show plots of the solutions at time $t = .5836$. The shear band is formed at $x = 0$ and it remains under plastic loading for the remainder of the numerical experiment. Two relief fronts expand from the shear band causing the material to unload. This is observed on the negative slope of the velocity in that region. The material remains under uniform loading in the region unaffected by the

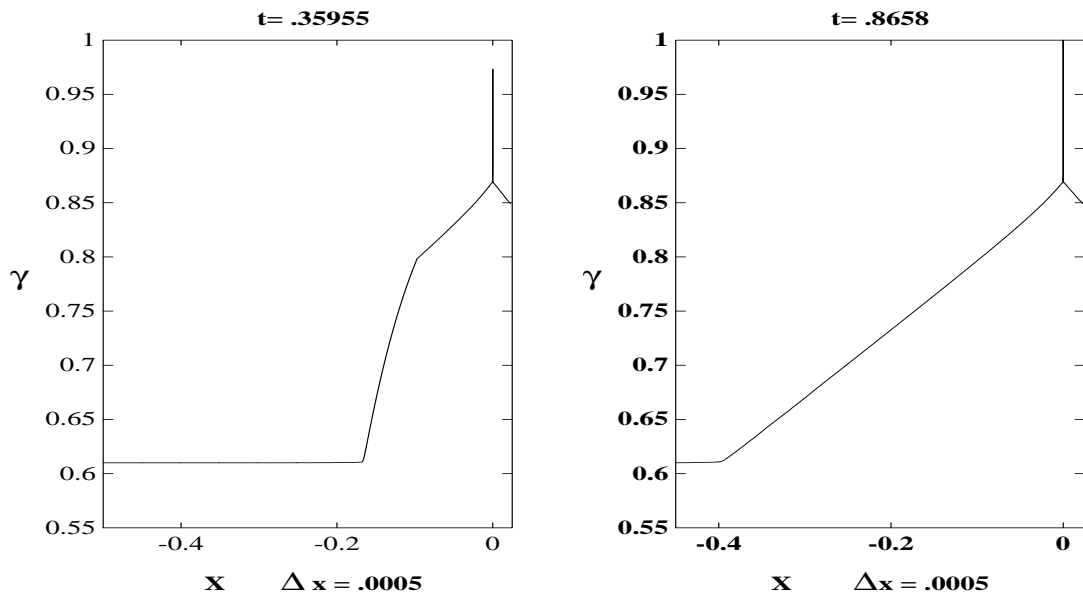


Figure 10: Yield Stress.

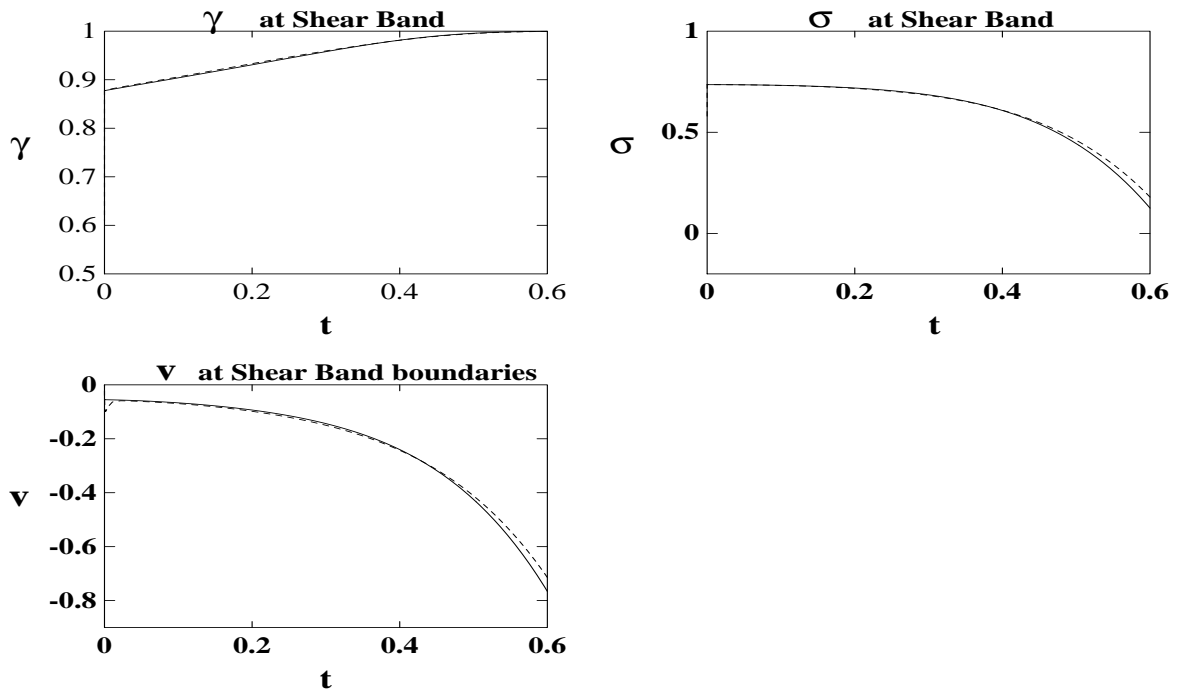


Figure 11: σ , u , γ at shear band.

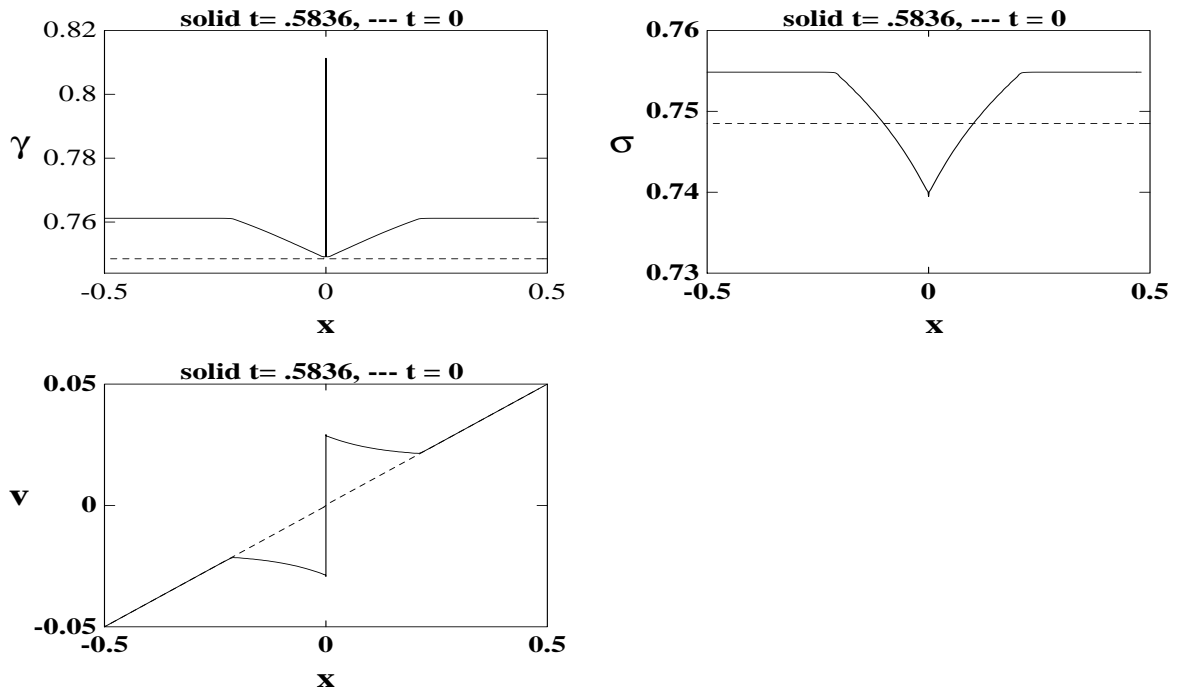


Figure 12: Uniform loading.

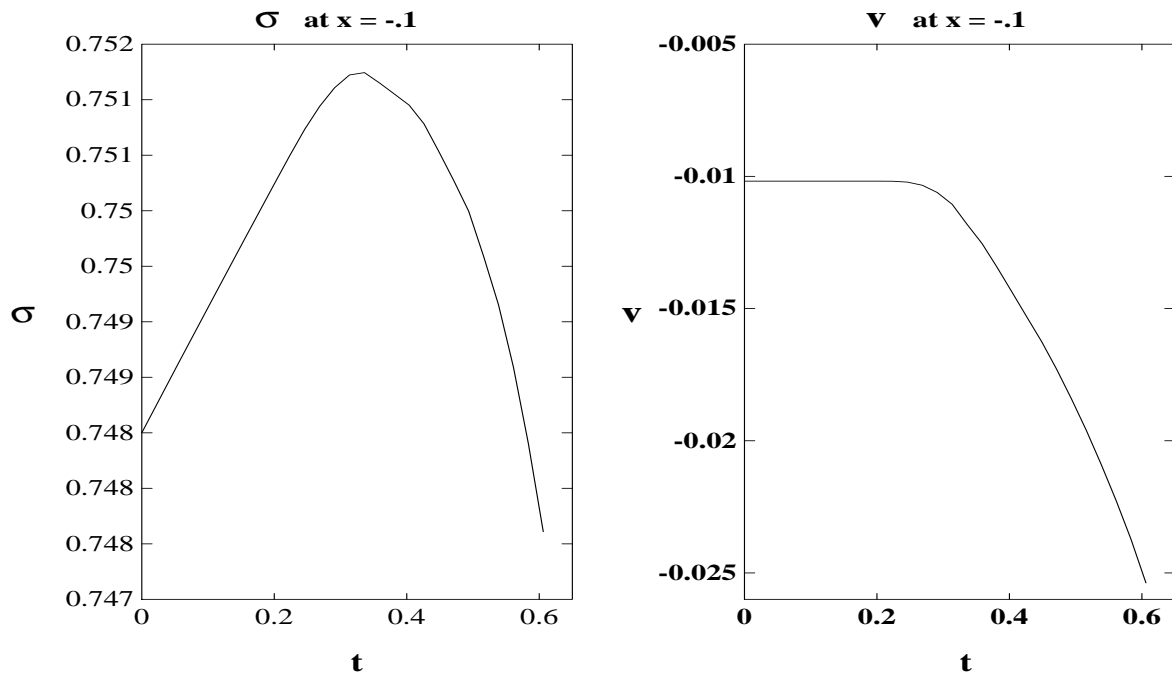


Figure 13: Solution at $x = -.255$.

relief front.

In Figure 13 we show the time evolution of the solution at a point away from the shear band ($x = -.1$). The material loads uniformly until $t \approx .3361$. At this time the relief front reaches the material point and the material unloads.

5.3 Uniform loading with two defects

The last numerical example consists of a uniform loading experiment on a sample with two unequal inhomogeneities. For a sample material as in the previous example, we introduce two inhomogeneities at $x = \pm .075$ by changing the value of α to $\alpha = .4975$ at $x = -.075$ and $\alpha = .5$ at $x = .075$. The initial data we impose is $\sigma(x, 0) = .745$, $\gamma(x, 0) = .745$, $\tau(x, 0) = 0$ and $(v(x, 0) = x/20)$. In this example two shear bands develop at $x = \pm .075$. Although initially both bands load plastically, eventually the interaction of the relief fronts for both bands forces the band with least amount of loading into elastic unloading (band at $x = .075$ for $t \geq 1.425$.) See Figure 14.

Between both shear bands, the material initially loads plastically, until reached by the relief front from the shear bands. After that it exhibits an oscillatory elastic unloading and loading until it goes into constant unloading.

In Figure 15 we show the time plots of the yield stress, normal stress and velocity jumps at both shear bands. The shear bands are loading while the velocity jumps remain positive. We also show a time plot of the normal stress at a point ($x = 0$) between the shear bands.

6 Appendix

A Bootstrap Method

In this section we describe a numerical algorithm for the solution of the Riemann problem stated in Section 3.2. This algorithm solves the system of ordinary differential equations (11), couple to the PDE, which is made implicit for σ_b , τ_b and γ_b in equation (35) below. This algorithm is used in Section 5.1 as a comparison for the numerical algorithm for the full system of partial differential equations (1)(2) as described in Section 4.

For simplicity in the exposition we consider the case of symmetric data, this is $\sigma_l = \sigma_r$, $\tau_l = \tau_r$, $\gamma_l = \gamma_r$ and $v_l = -v_r$. In this case the solution, as a function of x , will be even for the stresses and odd for the velocity. Assuming this symmetry of the solution, we only need to study the solution for $x > 0$.

SHEARER and SCHAEFFER (1993) prove the local existence of solutions to this problem when a classical selfsimilar solution does not exist. Along the way, they give

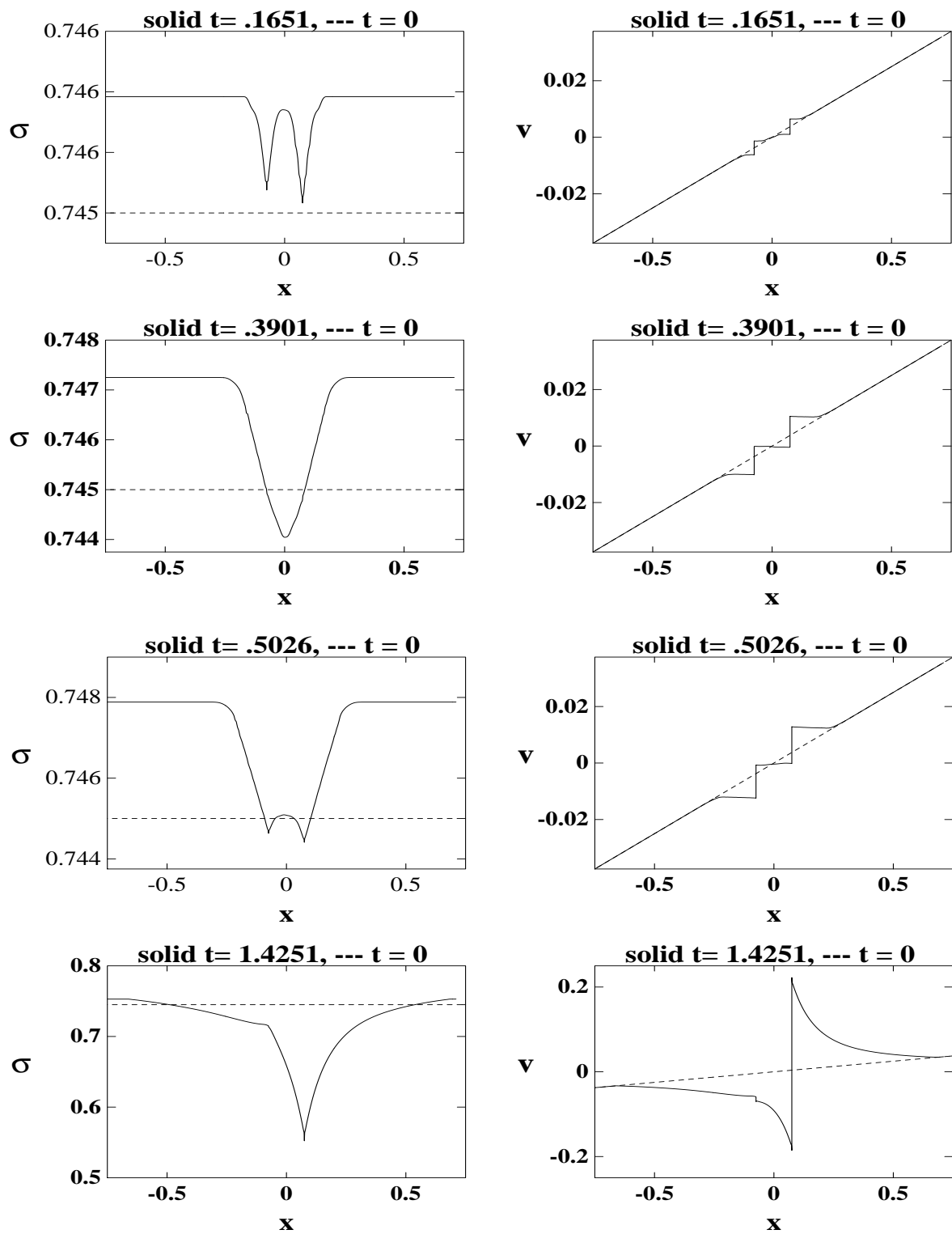


Figure 14: Two competing incipient shear bands. Snapshots at various times.

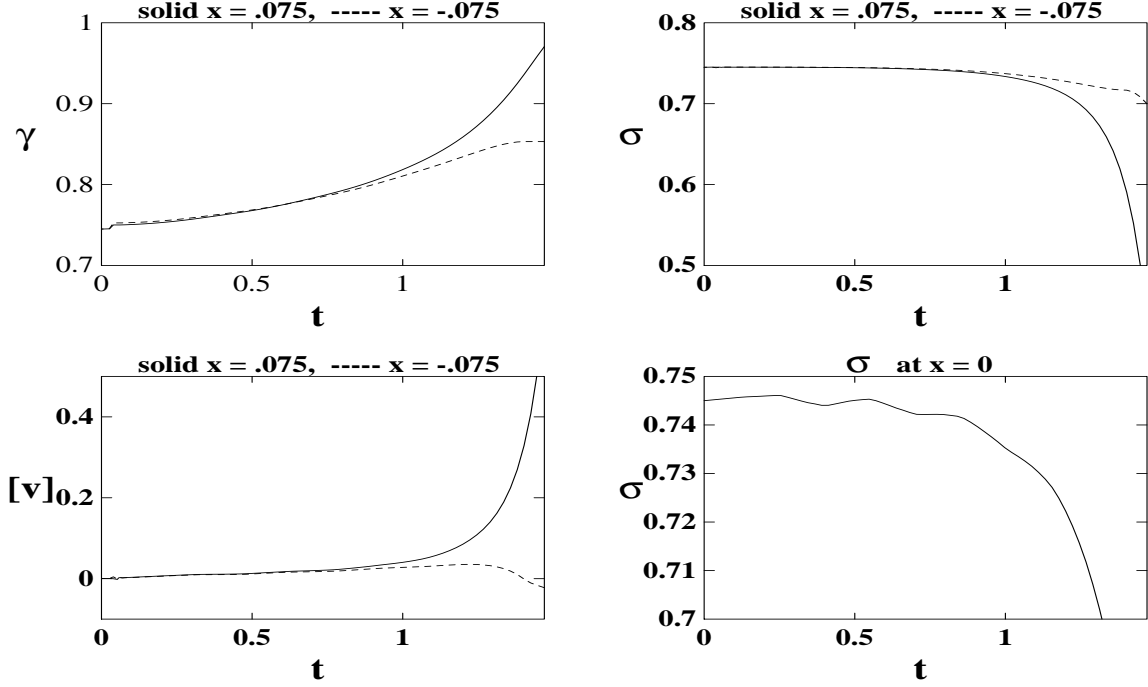


Figure 15: Two competing incipient shear bands. Time evolution at various locations.

a description of the asymptotic behavior of the relief front $x = s(t)$ for t small. We will use this description to initialize our algorithm.

With the notation of Section 3.2, we assume that the compatibility conditions $v_b(0) = \hat{v}(0)$, $\sigma_b(0) = \hat{\sigma}(0)$, $\tau_b(0) = \hat{\tau}(0)$ and $\gamma_b(0) = \hat{\gamma}(0)$ are satisfied; here $(\hat{v}, \hat{\sigma}, \hat{\tau}, \hat{\gamma})$ denotes the selfsimilar part of the solution. For this symmetric problem we write the evolution of the shear band (equation (11)) as

$$\frac{\partial}{\partial t} \begin{pmatrix} \sigma_b \\ \tau_b \\ \gamma_b \end{pmatrix} = \begin{pmatrix} 1 - \alpha^2 H'(\gamma_b) \\ \alpha H'(\gamma_b) \\ 1 \end{pmatrix} \frac{1}{1 + (1 - \alpha^2) H'(\gamma_b)} \frac{2v_{br}}{\delta}. \quad (31)$$

The solution to our initial value problem satisfies a linear system (13) on $\{t > 0, 0 < x < s(t)\}$ with nonlinear boundary conditions (31); it satisfies a nonlinear system (1)(2) on $\{t > 0, s(t) < x\}$; and it is continuous at $x = s(t)$ with the function $s(t)$ to be determined.

Next we describe the selfsimilar part of the solution for all $\xi > 0$. For the initial data $(v_r, \sigma_r, \tau_r, \gamma_r)$ we denote by $(v_r^1, \sigma_r^1, \tau_r^1, \gamma_r^1)$ the state connected to the initial data by a right moving elastic wave and lying on the elastic-plastic boundary, that is $\gamma_r^1 = \sigma_r^1 + \alpha \tau_r^1$ (see Figure 16). We define ξ_r^{max} as the eigenvalue associated to this state, $\xi_r^{max} = c\sqrt{\eta(\gamma_r^1)}$.

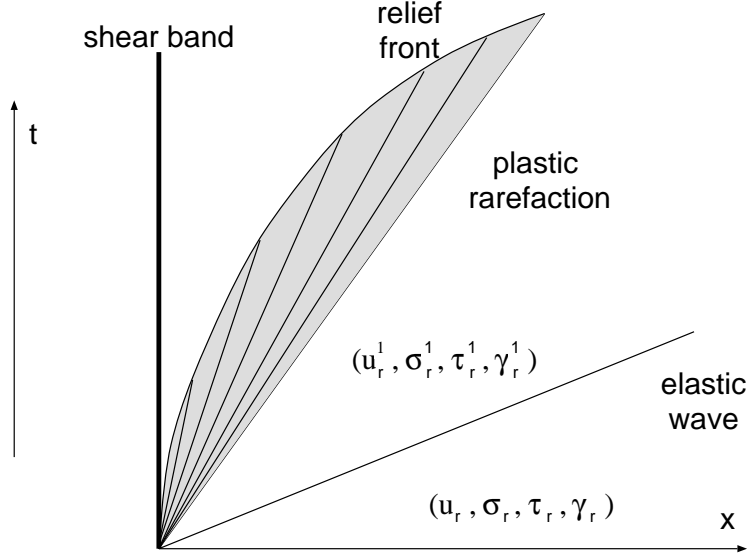


Figure 16: Relief front.

The selfsimilar part of the solution \hat{v} , $\hat{\sigma}$, $\hat{\tau}$ and $\hat{\gamma}$ may now be described in both the elastic and plastic loading regions. On the elastic region we have

$$\begin{aligned} \hat{v}(\xi) &= v_r, \hat{\sigma}(\xi) = \sigma_r, \hat{\tau}(\xi) = \tau_r \text{ and } \hat{\gamma}(\xi) = \gamma_r, \text{ for } \xi > c \\ \hat{v}(\xi) &= v_r^1, \hat{\sigma}(\xi) = \sigma_r^1, \hat{\tau}(\xi) = \tau^1 \text{ and } \hat{\gamma}(\xi) = \gamma_r^1, \text{ for } c \geq \xi \geq \xi_r^{max}. \end{aligned} \quad (32)$$

In the region where the plastic deformation takes place, $0 < \xi < \xi_r^{max}$, we write $(\hat{v}(\xi), \hat{\sigma}(\xi), \hat{\tau}(\xi), \hat{\gamma}(\xi))$ as the solution to the system of ordinary differential equations

$$\begin{aligned} \hat{v}_\xi &= \frac{2\xi^2(1 + (1 - \alpha^2)k(\hat{\gamma}))^3}{c^2 k'(\hat{\gamma})} \\ \hat{\sigma}_\xi &= \frac{-2\xi^3(1 + (1 - \alpha^2)k(\hat{\gamma}))^3}{c^4 k'(\hat{\gamma})} \\ \hat{\gamma}_\xi &= \frac{-2\xi(1 + (1 - \alpha^2)k(\hat{\gamma}))^2}{c^2 k'(\hat{\gamma})} \end{aligned} \quad (33)$$

with $\hat{\tau}(\xi) = (\hat{\gamma} - \hat{\sigma})/\alpha$ and continuous at $\xi = \xi_r^{max}$. This completes the description of the selfsimilar part of the solution.

Next we describe, with the help of the Riemann invariants, the relation between the states at the shear band and the states at the relief front. In the elastic unloading region $\{t > 0, 0 \leq x \leq s(t)\}$, next to the shear band, the solution satisfies a linear wave equation. In this region, the Riemann invariants are $R_+(x, t) = v(x, t) - c\sigma(x, t)$, and $R_-(x, t) = v(x, t) + c\sigma(x, t)$. Along the characteristic lines, these invariants

satisfy

$$\begin{aligned} R_-(x, t) &= R_-(x_0, t_0) & \text{for } x &= x_0 - c(t - t_0) \\ R_+(x, t) &= R_+(x_0, t_0) & \text{for } x &= x_0 + c(t - t_0). \end{aligned} \quad (34)$$

Lemma A.1 *We assume that the position of the relief front, $s(t)$, is known for $t \leq t_f$ for some given $t_f > 0$. Then v_{br} , σ_b , τ_b and γ_b are determined for $t \leq t_b = t_f + s(t_f)/c$.*

Proof. From the equation (34a), $R_-(0, t) = v_{br}(t) + c\sigma_b(t) = R_-(c(t - t_r), t_r)$ while $c(t - t_r) \leq s(t_r)$. (See Figure 17.) We solve this equation for v_{br} when $c(t - t_r) = s(t_r)$ and $t_r \leq t_f$

$$v_{br}(t_r + s(t_r)/c) = -c\sigma_b(t_r + s(t_r)/c) + \hat{v}(s(t_r)/t_r) + c\hat{\sigma}(s(t_r)/t_r).$$

Now equation (31) is expressed as an implicit ordinary differential equation

$$\frac{\partial}{\partial t} \begin{pmatrix} \sigma_b \\ \tau_b \\ \gamma_b \end{pmatrix} = \begin{pmatrix} 1 - \alpha^2 H'(\gamma_b) \\ \alpha H'(\gamma_b) \\ 1 \end{pmatrix} \frac{1}{1 + (1 - \alpha^2) H'(\gamma_b)} \frac{2\Sigma(t, \sigma_b)}{\delta}. \quad (35)$$

where

$$\Sigma(t, \sigma_b) \equiv \hat{v}(x_r/t_r) + c\hat{\sigma}(x_r/t_r) - c\sigma_b(t) \quad (36)$$

and (x_r, t_r) is the solution, for each t , to the algebraic system $x_r = c(t - t_r)$ and $x_r = s(t_r)$ for $0 \leq t \leq t_b$. ■

Lemma A.2 *We assume that the states $(v_{br}, \sigma_b, \tau_b, \gamma_b)$ on the shear band are known for $0 \leq t \leq t_b$ for some given $t_b > 0$. We also assume that the position of the relief front, $s(t)$, is known for $0 \leq t \leq t_f$ for some given t_f , $0 < t_f \leq t_b$. Then the position of the relief front can be determined for values of $t \leq t_b + \epsilon$ for some $\epsilon > 0$.*

Proof. From equation (34b) $R_+(0, t_0) = v_{br}(t_0) - c\sigma_b(t_0) = R_+(c(t - t_0), t)$ while $c(t - t_0) \leq s(t)$. If we write $\xi = c(t - t_0)/t$, the intersection of the right characteristic $x = c(t - t_0)$ with the relief front is given by the solution to the equation

$$R_+(0, t_0) = \hat{v}(\xi) - c\hat{\sigma}(\xi). \quad (37)$$

From (33) we notice that

$$(\hat{v} - c\hat{\sigma})_\xi = \frac{2\xi^2(1 + (1 - \alpha^2)k(\hat{\gamma}))^3}{c^2 k'(\hat{\gamma})} \left(1 + \frac{\xi}{c}\right) \geq 0.$$

Therefore the uniqueness of the solution ξ to (37) is guaranteed. We notice that $R_+(0, t)$ is an increasing function of t (in the notation of Appendix B, equation (48),

$(R_+(0,t))' = F'(t) \geq 0$); thus $\xi = \xi(t_0)$, the solution to equation (37), is also an increasing function. The existence of such solution is guaranteed as far as the relief front does not reach the leading edge of the plastic rarefaction. After that point, the relief front travels at elastic speed c .

The solution ξ_0 to equation (37) determines the ray $x = \xi_0 t$ on which the intersection of the right characteristic line $x = c(t - t_0)$ and the relief front lies. This point is given by $t = ct_0/(c - \xi_0)$ and $x = ct_0\xi_0/(c - \xi_0)$ for $t_0 \leq t_b$.

From the monotonicity of $\xi = \xi(t_0)$ we have that for any $t_0 \leq t_b$ $\xi(t_0) > s(t_f)/t_f$. Therefore, for $t_0 \leq t_b$, the corresponding point on the relief front satisfies

$$t = \frac{ct_0}{c - \xi(t_0)} \geq \frac{ct_f}{ct_f - s(t_f)} t_0 = \left(1 + \frac{s(t_f)}{ct_f - s(t_f)}\right) t_0.$$

Setting $t_0 = t_b$ in the above equation, proves the lemma with $\epsilon = \frac{t_b s(t_f)}{ct_f - s(t_f)}$. ■

Now, exploiting the above two lemmas, we present an algorithm which constructs

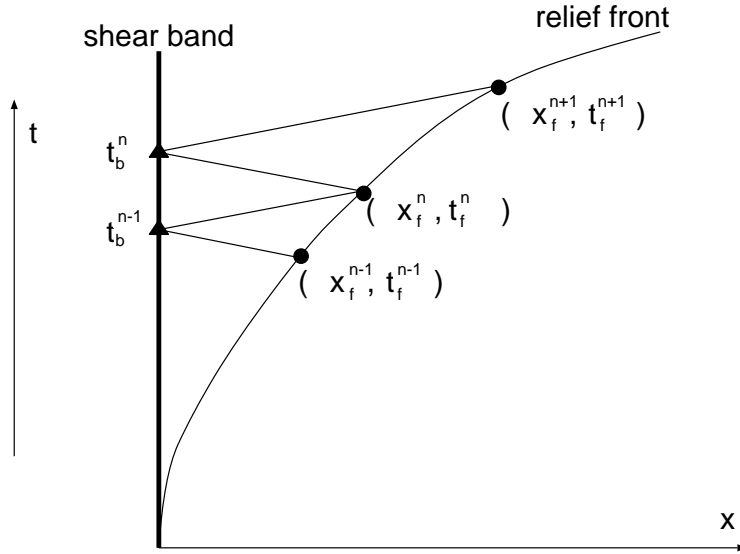


Figure 17: Bootstrap.

the solution on the shear band and determines the location of the relief front $x = s(t)$. We denote the points on the shear band by $(0, t_b)$ and the points on the relief front by (x_f, t_f) . The algorithm is described in three steps:

- (i) Initialization We write $t_b^0 = t_f^0 = x_f^0 = 0$. Our choice of (x_f^1, t_f^1) is based on the asymptotic approximation of the relief front offered by SCHAEFFER and SHEARER (1993). In this paper they show that the relief front is asymptotic to the line $x = 0$ at the origin and, for small values of t , it behaves like $s(t) = Ct^{3/2} + O(t^2)$ with $C = c^{7/4} \frac{\alpha^3}{3^{1/4}} (\frac{2v_0}{\delta} k'(\gamma_0))^{1/2}$. Here $v_0 = \hat{v}(0)$ and $\gamma_0 = \hat{\gamma}(0)$. We choose a small value for t_f^1 and x_f^1 is then given by this asymptotic approximation, $x_f^1 = C(t_f^1)^{3/2}$.
- (ii) Updating of the shear band from the relief front. We assume that the solution on the shear band is known at a time t_b^{n-1} as well as two points (x_f^{n-1}, t_f^{n-1}) and (x_f^n, t_f^n) on the relief front satisfying $t_b^{n-1} = t_f^{n-1} + x_f^{n-1}/c$ and $t_f^n > t_f^{n-1}$. First we approximate the relief front linearly between these two points: i.e., $t_f^{n-1} \leq t \leq t_f^n$ we write

$$s(t) = x_f^{n-1} + \frac{x_f^n - x_f^{n-1}}{t_f^n - t_f^{n-1}}(t - t_f^{n-1}). \quad (38)$$

We use Lemma A.1 to evaluate σ_b , τ_b , γ_b and v_{br} for $t_b^{n-1} < t \leq t_b^n$ where $t_b^n = t_f^n + x_f^n/c$ is such that the point $(0, t_b^n)$ is on the left characteristic line passing through (x_f^n, t_f^n) .

- (iii) Updating of the relief front from the shear band We use Lemma A.2 to determine a new point (x_f^{n+1}, t_f^{n+1}) on the relief front which also lies on the right characteristic line through $(0, t_b^n)$, $x = c(t - t_b^n)$.

We iterate steps (ii) and (iii) until the relief front overtakes the leading edge of the rarefaction wave (the ray $x = \xi_r^{max} t$.) This completes the description of the "bootstrap" algorithm.

B Global properties for the Riemann problem with a shear band

In the course of this research, we were able to prove that the symmetric Riemann problem for the initiation of a shear band (cf. Section 3.2) admits a global solution. This generalizes the local existence result of SCHAEFFER and SHEARER (1993). We prove this result here and also include some remarks on the asymptotic behavior of the free boundary as $t \rightarrow +\infty$.

We start with (a slight modification of) the formulation ((2.4) of SCHAEFFER and SHEARER (1993)) of the problem as a functional/integral equation. It is necessary

to find three functions F , G , and r of one variable t , r being nonnegative and satisfying $r(0) = 0$, such the for $t \geq 0$

$$\begin{aligned} \text{(a)} \quad F + G \circ \phi &= \hat{v}(r) \\ \text{(b)} \quad F - G \circ \phi &= -\hat{\sigma}(r) \\ \text{(c)} \quad F - G &= -b(\int_0^t (F + G) dt') \end{aligned} \tag{39}$$

where

$$\phi(t) = \frac{1 - r(t)}{1 + r(t)} t \tag{40}$$

and \hat{v} , $\hat{\sigma}$ and b are data functions with the behavior sketched in Figure 18. The salient features of the graphs are:

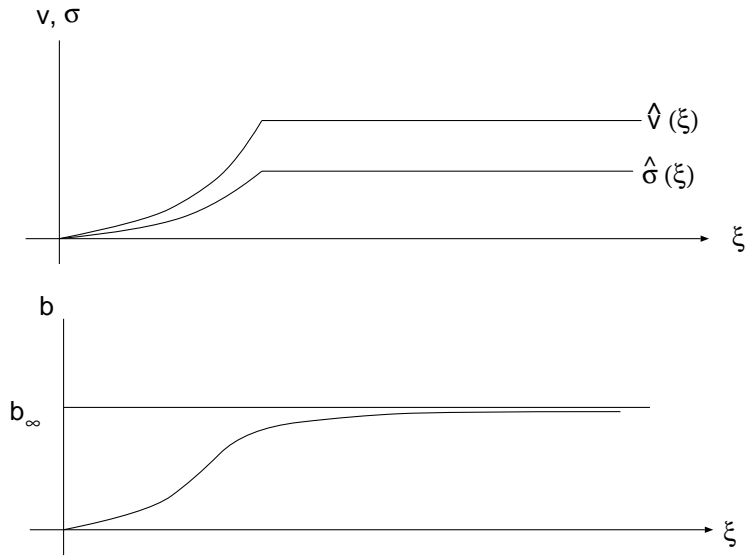


Figure 18: The data functions in (39).

Property A: For $0 \leq \xi < \xi_0$, the derivatives satisfy

$$0 < \hat{\sigma}'(\xi) < \hat{v}'(\xi)$$

and are increasing functions.

Property B: $\hat{v}(0)$ and $\hat{\sigma}(0)$ vanish, and for $\xi \geq \xi_0$ both functions are constant.

Property *C*: The function b is strictly increasing.

These properties are derived in SCHAEFFER and SHEARER (1993). In fact equation (39) differs slightly from (2.4) of (39) in that here we have (i) changed the sign of $\hat{\sigma}$ and of b to obtain positive quantities and (ii) rescaled the variables so that the constants v_0 and σ_0 of (2.8) in SCHAEFFER and SHEARER (1993) both vanish. Also, the extension of \hat{v} and $\hat{\sigma}$ to values of the argument greater than ξ_0 is a minor generalization of SCHAEFFER and SHEARER (1993). The extension derives from the fact that ahead of rarefaction waves the solution is constant. Finally, in Figure 18 the graph of $b(\xi)$, as drawn, asymptotes to a constant value as $\xi \rightarrow \infty$. This is the most realistic behavior, and it is exhibited by the full model of SCHAEFFER and SHEARER (1993). For the simplified model of the present paper, the function $b(\xi)$ actually tends to infinity as $\xi \rightarrow \infty$. However, this asymptotic behavior does not affect the global existence result given here. (It does affect the qualitative properties of the solution as $t \rightarrow \infty$).

The functions F , G and r relate to the unknowns of the present paper as follows: We are assuming symmetric data (i.e., v odd in x , σ even), so it suffices to confine our attention to the half space $\{x \geq 0\}$. Material is unloading in a region adjacent to the shear band at $x = 0$ and described by

$$\{(x, t) : t > 0, 0 < x < s(t)\} \quad (41)$$

where $s(t)$ relates to $r(t)$ by

$$r \circ \psi(t) = \frac{s(t)}{t} \quad (42)$$

where $\psi(t) = t + s(t)$. For future reference we notice that from the comment after (2.6) in SCHAEFFER and SHEARER (1993) we also have

$$\psi^{-1}(t) = \frac{t}{1 + r(t)} \quad (43)$$

Within the unloading region (41), the velocity and stress are given by

$$\begin{aligned} \text{(a)} \quad v(x, t) &= F(t + x) + G(t - x) \\ \text{(b)} \quad \sigma(x, t) &= F(t + x) - G(t - x) \end{aligned} \quad (44)$$

(For this appendix we have scaled x and t so that the wave speed c equals unity.) The functions \hat{v} and $\hat{\sigma}$ specify the velocity and normal stress in the rarefaction wave adjacent to the unloading region, and b specifies the evolution of the shear band obtained by integrating (9).

To explain the idea of the existence proof, we rearrange equations (39) as follows:

$$\begin{aligned}
 \text{(a)} \quad 2F(t) &= (\hat{v} - \hat{\sigma})(r(t)) \\
 \text{(b)} \quad 2G\left(\frac{1-r(t)}{1+r(t)}t\right) &= (\hat{v} + \hat{\sigma})(r(t)) \\
 \text{(c)} \quad G(t) &= F(t) + b\left(\int_0^t (F + G)dt'\right)
 \end{aligned}
 \tag{45}$$

Suppose that we have a solution of (45) for $0 \leq t \leq t_0$. (We know from SCHAEFFER and SHEARER (1993) that (45) admits a solution on some positive time interval.) The key observation is that, since $r(t)$ is a positive quantity, the argument of G on the LHS of (45b) is strictly less than t_0 for all t in $[0, t_0]$. Therefore, at least for values of t slightly larger than t_0 , one may write an equation for $r(t)$ that involves the unknown function G but only for arguments in the interval $[0, t_0]$ where G has already been determined; viz,

$$2G\left(\frac{1-r(t)}{1+r(t)}t\right) = (\hat{v} + \hat{\sigma})(r(t)). \tag{46}$$

We will show that for each t in some interval $[0, t_0 + \epsilon]$, equation (46) may be solved for the scalar variable r . In this way we extend $r(t)$ to a larger interval. Given $r(t)$, we may extend F to the larger interval with (45a), and by solving the nonlinear Volterra equation (45c), we may also extend G .

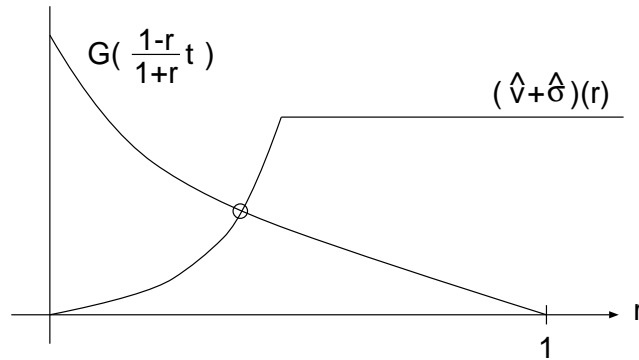


Figure 19: Numerical solution of equation (46).

The above discussion provides the framework for the proof that (45) admits a global solution; it remains to show that (46) may be solved as claimed. We will show this graphically with the aid of Figure 19 in which both sides of equation (46) are plotted. Substituting $t = 0$ in (45b), we see that $G(0) = 0$; therefore the LHS of (46) vanishes at $r = 1$. It follows from the next lemma that the LHS of (46) is positive at

$r = 0$ and that the LHS is a monotone function of r (decreasing since $(1-r)/(1+r)$ is decreasing). Therefore, as illustrated in Figure 19, the equation admits a unique solution.

Before beginning in earnest, let us prove that $r(t) < 1$. Basically this is a consequence of the fact that the free boundary propagates slower than the elastic speed $c = 1$, so that $s(t) < t$. However in our proof we must compensate for the reparametrization of time by $\psi(t)$ in (42). If $r(t)$ were not always strictly less than 1, then there would be a time t_* such that $r(t_*) = 1$. By (43), $\psi^{-1}(t_*) = t_*/2$. Then from (42)

$$\frac{s(t_*/2)}{t_*/2} = r(\psi(t_*/2)) = r(t_*) = 1,$$

a contradiction.

Lemma B.1 *If (45) admits a solution F, G, r on $[0, t_0]$, then all three functions are monotone increasing on this interval.*

Proof. We differentiate (45) and rearrange terms in (45b) to obtain:

$$\begin{aligned} \text{(a)} \quad 2F'(t) &= (\hat{v} - \hat{\sigma})'(r(t))r'(t) \\ \text{(b)} \quad 2\frac{1+r(t)}{1-r(t)}G'(\frac{1-r(t)}{1+r(t)}t) &= \left\{ (\hat{v} + \hat{\sigma})'(r(t)) + \frac{4t}{(1-r)^2}G'(\frac{1-r(t)}{1+r(t)}t) \right\} r'(t) \\ \text{(c)} \quad G'(t) &= F'(t) + b'(\int_0^t (F+G)dt')(F+G)(t) \end{aligned} \quad (47)$$

The small-time solution of (45b) that is constructed in SCHAEFFER and SHEARER (1993) satisfies

$$\begin{aligned} \text{(a)} \quad F'(t) &\geq 0 \\ \text{(b)} \quad G'(t) &> 0 \\ \text{(c)} \quad r'(t) &> 0 \end{aligned} \quad (48)$$

for $0 \leq t < \epsilon$. Suppose (48) is satisfied for $0 \leq t < t_*$. On observing that for all t in some interval $[0, t_* + \epsilon]$ the argument of G' in (47b) is still smaller than t_* , we conclude from (48b) and Property *A* that $r'(t)$ is positive on $[0, t_* + \epsilon]$. Then we conclude from (47c), (48a), and Property *C* that $G'(t_*) > 0$ and hence by continuity $G'(t)$ is also positive on some larger time interval. Finally we conclude from (47a) and Properties *A* and *B* that $F'(t)$ is nonnegative on a larger interval. This completes the proof. ■

Finally we briefly examine the asymptotic behavior of the global solution as $t \rightarrow \infty$. By the lemma, $r(t)$ is a monotone increasing function, therefore $r(t)$ tends to some limit $r_\infty \leq 1$ as $t \rightarrow \infty$. The case $r_\infty = 1$ occurs whenever, as illustrated in Figure 20b, the relief wave overtakes the leading edge of the rarefaction wave. Indeed, after the time of overtaking, the relief wave propagates with the elastic wave speed

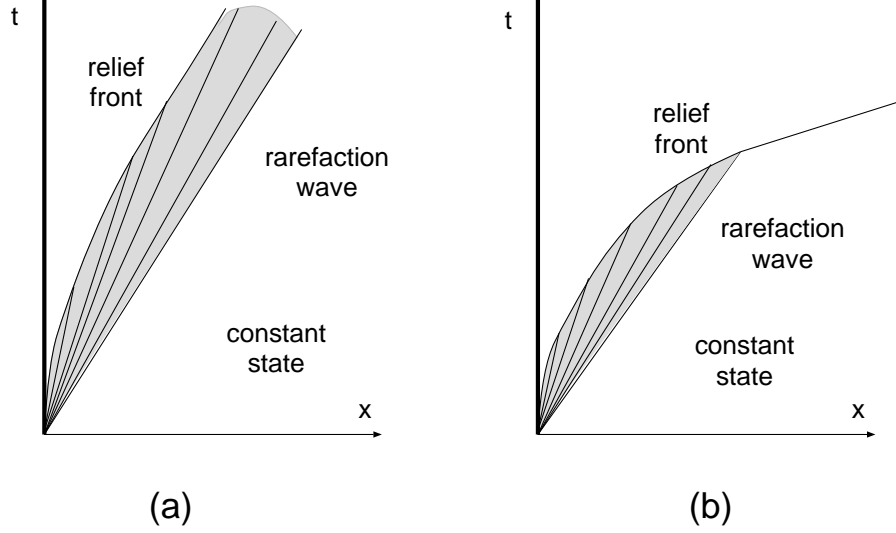


Figure 20: Two possible asymptotic states.

$c = 1$ so that $s(t) = t - k$ for some constant k and $r(t) = 1 - k/t$. In case $r \rightarrow r_\infty < 1$, let $F(t)$ and $G(t)$ approach limits F_∞ and G_∞ as $t \rightarrow \infty$. Observe that

$$G \circ \phi \approx G\left(\frac{1 - r_\infty}{1 + r_\infty}t\right)$$

also tends to the limit G_∞ . By (39), these limits must satisfy

$$\begin{aligned} \text{(a)} \quad F_\infty(t) + G_\infty(t) &= \hat{v}(r_\infty) \\ \text{(b)} \quad F_\infty(t) - G_\infty(t) &= -\hat{\sigma}(r_\infty) \\ \text{(c)} \quad F_\infty(t) - G_\infty(t) &= -b_\infty. \end{aligned} \tag{49}$$

These equations admit a solution (which is unique) if and only if there is a value r_∞ such that

$$\hat{\sigma}(r_\infty) = b_\infty, \tag{50}$$

which puts a lower limit on the strength of the rarefaction wave: It must be greater than b_∞ , the decrease in normal stress at the shear band in the limit of infinite shearing. For the model of the present paper in which $b_\infty = \infty$, equation (50) never has a solution; i.e., the relief wave always overtakes the leading edge of the rarefaction wave.

References

- CHERN, I-L. and COLELLA, P. (1987) A conservative front tracking method for hyperbolic conservation laws. Technical Report UCRL-97200, Lawrence Livermore National Laboratory, Lawrence Livermore National Laboratory, Berkeley, CA 94720, July 1987.
- CLIFTON, R. J. and BODNER, S. R. (1965) An analysis of longitudinal elastic-plastic pulse propagation. *J. of Applied Mechanics* , **65**, 1-8.
- CLIFTON, R. J. and TING, T. C. T. (1968) The elastic-plastic boundary in one-dimensional wave propagation. *J. of Applied Mechanics* , **35**, 812-814.
- GARAIZAR, X. (1993) Numerical computations for antiplane shear in a granular flow model. *Quarterly of Applied Mathematics*, to appear.
- VON KARMAN, TH. , BOHNENBLUST, H. F. and HYERS, D. H. (1943) The propagation of plastic waves in tension specimens of finite length. *NDRC Report #A-103*, OSRD #946.
- LEE, E. H. (1953) A boundary value problem in the theory of plastic wave propagation. *Quarterly of Applied Mathematics* , **10**, 335-346.
- MANDEL, J. (1964) Conditions de stabilite et postulate de Drucker. *Rheology and Soil Mechanics, IUTAM Symposium at Grenoble* (ed. G. Kravtchenko and P. Sirieys), 58-68.
- RAKHMATULIN, KH. A. (1945) On propagation of the unloading wave. *Prikladnaya Matematika i Mekhanika* , **9**, 91-100.
- SCHAEFFER, D. G. (1990) Instability and ill-posedness in the deformation of granular materials. *International Journal for Numerical Analysis Methods Geomechanics*, **14**, 253-278.
- SCHAEFFER, D. G. (1992) A mathematical model for localization in granular flow. *Proceedings of the Royal Society of London*, **436**, 217-250.
- SCHAEFFER, D. G. and SHEARER, M. (1993) Unloading near a shear band: A free boundary problem for the wave equation. *Comm. in PDE*, to appear.
- SHEARER, M. and SCHAEFFER, D. G. (1993) Unloading near a shear band in granular material. *Quarterly of Applied Mathematics*, to appear.
- SKOBEEV, A. M. (1963) On the theory of unloading waves. *Applied Mathematics and Mechanics* , PMM **26**, 1605-1615. TRANGENSTEIN J. A. and PEMBER R. B. (1992) Numerical algorithms for strong discontinuities in elastic-plastic solids. *J. Comp. Phys.*, to appear.